ASTROBIOLOGY
Volume 9, Number 8, 2009

DOI: 10.1089/ast.2008.0263

**Research Article**

# Microbial Dissolution of Hematite and Associated Cellular Fossilization by Reduced Iron Phases: A Study of Ancient Microbe-Mineral Surface Interactions

Kamal Kolo,[1] Kurt Konhauser,[2] Wolfgang Elisabeth Krumbein,[3] Yves Van Ingelgem,[4] Annick Hubin,[4] and Philippe Claeys[1]

**Abstract**

We report here on magnetite- and wustite-encrusted and geometrically oriented microbial-like structures (MLS) attached to the surfaces of hematite ($\alpha$-$Fe_2O_3$) crystals in a banded iron formation. Field emission scanning electron microscope (FE-SEM) and scanning electron microscope (SEM) imaging showed a 3-D network of MLS arranged in $1\,\mu m \times \sim 20\,\mu m$ coccoidal-like chains (CLC) of various geometrical shapes: dichotomous and budding-like protrusions, parallel, intersecting, triangular, or sinusoidal. Individual spheroidal forms ($\sim 1\,\mu m$ in diameter), some displaying what appears to be division, were also abundant. In addition to their size, morphology, and preferred orientations, a microbial origin of these chains and single spheroidal forms is inferred by the presence of material that resembles extracellular polymeric substances (EPS) extending from the base of the chains along the mineral surface: the attachment sites show circular dissolution pits of about 100 nm diameter. Other thin structures protruding from the CLC are reminiscent of bacterial "nanowires." We were, however, unable to find any extant cells, organic carbon, or even recover DNA from the MLS, which suggests that they, if microbial, are possibly mineralogically replaced casts or mineral encrustations of cells. It is further speculated that, given the nature of the substrate upon which the forms are attached and their preferential orientations, it seems plausible that the "original cells" may have been Fe(III)-reducing bacteria that exploited structural imperfections in the crystal lattice. Importantly, the preservation of the ancient microbial shapes in mineral casts of magnetite, wustite, or both may be an overlooked means by which cellular features in the rock record are retained. Key Words: Bacteria—Banded iron formation—Microbe-mineral interactions—Iron-reducing bacteria—Microbial fossils—Cellular fossilization. Astrobiology 9, 777–796.

## Introduction

Bacteria can use iron as a source of energy, and their roles as Fe(II) oxidizers or Fe(III) reducers are well described in modern environments (*e.g.,* Lovely and Phillips, 1988; Lovley, 1991; Lovley *et al.*, 1992, 1993, 2004; Roden and Lovley, 1993; Bazylinski *et al.*, 1995; Lonergan *et al.*, 1996; Bazylinski and Moskowitz, 1997; Kieft *et al.*, 1999; Chaudhuri *et al.*, 2001; DiChristina *et al.*, 2002, 2005; Nevin and Lovley, 2002; Bazylinski and Frankel, 2003; Frankel and Bazylinski, 2003). Bacterial cycling of Fe was also likely an important process on early Earth. In the case of the oxidative reactions, Fe(II)-oxidizing phototrophs in the Archean and Paleoproterozoic oceans have been linked to the deposition of banded iron formations (BIF) (Konhauser *et al.*, 2002a; Kappler *et al.*, 2005; Canfield *et al.*, 2006). The formation of iron hydroxides, $Fe(OH)_3$, by phototrophic bacterial oxidation of dissolved Fe(II) has recently been experimentally validated with several species of purple non-sulfur, purple sulfur, and green sulfur bacteria (*e.g.,* Kappler and Newman, 2004; Kappler *et al.*, 2005) and by the finding of a Fe(II)-oxidizing bacterium capable of directly forming magnetite and goethite (Jiao *et al.*, 2005). Furthermore, the Fe isotope record in early Archean rocks suggests that incomplete oxidation of marine $Fe^{2+}_{aq}$ could have

[1]Earth System Science and [4]Research Group Electrochemical and Surface Engineering, Department Materials and Chemistry, Vrije Universiteit Brussel, Brussels, Belgium.
[2]Department of Earth and Atmospheric Sciences, University of Alberta, Edmonton, Alberta, Canada.
[3]Geomicrobiology, ICBM, Carl-von-Ossietzky Universität Oldenburg, Oldenburg, Germany.

occurred by anaerobic photosynthetic Fe(II) oxidation, which produced Fe(III) oxides in BIF with positive $\delta^{56}$ Fe values (Johnson *et al.,* 2008a), similar to experimental results with Fe(II)-oxidizing phototrophs (Croal *et al.,* 2004).

With regard to ancient reductive processes, there is putative evidence for the presence of dissimilatory Fe(III)-reducing bacteria (DIRB) that coupled the reduction of ferric iron minerals to the oxidation of cell biomass (Lovley and Phillips, 1988; Lovley *et al.,* 2004). This evidence comes from (1) the Fe isotope record in BIF that show highly negative $\delta^{56}$ Fe values in magnetite grains that closely mimic those observed during modern dissimilatory Fe(III) reduction (*e.g.,* Johnson *et al.,* 2008a, 2008b); (2) microbial ecological studies that have shown that the deepest-branching Bacteria and Archaea are capable of Fe(III) reduction (Vargas *et al.,* 1998); and (3) petrographic analyses of BIF samples that showed the presence of secondary magnetite (Ewers and Morris, 1981). Recently, Konhauser *et al.* (2005) estimated that, during BIF deposition in the Archean–early Paleoproterozoic, nearly 70% of the biologically formed Fe(III) could have been recycled back into the water column via fermentation and organic carbon oxidation coupled to microbial reduction of the initial ferric hydroxide precipitates.

There are three mechanisms by which bacteria reduce ferric iron minerals. The first involves dissolution of Fe(III) oxides by high-affinity Fe(III) chelators and subsequent reduction of the chelated Fe(III) at the surface of, or within, the DIRB (Lovley and Phillips, 1988; Das and Caccavo, 2001; Caccavo and Das, 2002; DiChristina *et al.,* 2002; Nevin and Lovley, 2002; Lovley *et al.,* 2004; Neal *et al.,* 2005). The second involves exogenous humic or endogenous quinone substances that can serve as soluble electron shuttles between Fe(III)-reducing microorganisms and Fe(III) oxides (Newman and Kolter, 2000). The third necessitates direct adhesion to the mineral surface and is thought to occur within the cell-oxide interfacial area (Lovley *et al.,* 2004). In this mechanism, electrons are shuttled from a reduced source within the cytoplasm across the plasma membrane and periplasm to the outer membrane where they are then transferred directly to Fe(III) in the crystal structure, which causes a weakening of the iron-oxygen bond and reductive dissolution of the mineral (Lower *et al.,* 2001). Indeed, this mechanism appears the most utilized by several types of DIRB, such as *Geobacter metallireducens*, *Shewanella algae* BrY, *S. putrefaciencs,* and *S. oneidensis* (Caccavo *et al.,* 1997; Little *et al.,* 1997; Lower *et al.,* 2001; Caccavo and Das, 2002). Recently, another pathway of extracellular electron transfer has been proposed, which includes the microbial appendages known as "nanowires" that conduct electrons to the mineral surface (Childers *et al.,* 2002; Reguera *et al.,* 2005; Gorby *et al.,* 2006).

In any of the mechanisms above, to access a Fe(III) source, the chemoheterotrophic bacteria must be able to recognize the Fe(III) mineral surface and attach to it, as well as have the capability to activate or produce proteins that interact with that mineral surface (Konhauser, 2007). Some Fe(III)-reducing species, such as *G. metallireducens,* access insoluble Fe(III) oxides specifically by expressing pili and flagella to search and establish contact with the insoluble oxides (Childers *et al.,* 2002). However, only a few studies have highlighted the possibility of bacterial recognition and adhesion to a specific mineral surface, that is, the selective adherence of *S. oneidensis* to (010) surface of goethite ($\alpha$-FeOOH) compared to diaspore (AlOOH) (Lower *et al.,* 2001). A biased bacterial alignment parallel to ⟨110⟩ and ⟨100⟩ crystallographic directions has also been observed on sulfide minerals (pyrite, marcasite, and arsenopyrite) (Edwards *et al.,* 1998, 1999, 2000; Edwards and Rutenberg, 2001). Collectively, these arguments suggest that bacteria could produce oriented growth forms that are guided by mineral substrate chemistry and crystallography.

Therefore, the objectives of this study were to report, through field emission scanning electron microscope (FE-SEM), scanning electron microscope X-ray detector (SEM-EDX), and field emission auger electron spectrometer (FE-AES) imaging and analysis, on microbial-like structures (MLS) found on hematite surfaces from BIF in the Kasai region of Zaire, which display strong morphological similarities with microbial forms and are selectively adhered to the mineral surfaces. These MLS are mineralogically composed of magnetite and wustite and have crystallographically oriented coccoidal-like and chain growth patterns that display appendages. In this study, and due to a lack of further direct evidence, we present and discuss these MLS as possible remnants of ancient Fe(III)-reducing bacteria that were fossilized as a consequence of their chemoheterotrophic activity.

## Materials and Methods

### *Hematite samples*

Hematite ($\alpha$-$Fe_2O_3$) samples were acquired from the collection at the Earth System Science, Vrije Universiteit Brussel. The samples represent portions of a block of specular hematite (~3.5 kg) from the remineralized BIF of Kasai area, Zaire. The main BIF ore body is situated around the coordinates 5°30′S and 21°15′ E within the confluence area of Kasai and Lulua rivers, as described in the mineralogical and geological database of the Geological Research Institute/Royal Museum of Central Africa-Brussels. The database on the BIF of Kasai area is poor. The studies of INGA-INDUSTRIES (1968) and Raucq (1969) are the only known studies of BIF of this area. The pressure-temperature constraints and metallogeny of BIF in this area are still unstudied. Surface excavations, drilling, and magnetic survey have shown that the ore occurs as several separate, relatively small, but adjacent, ore bodies of low grade ~38% Fe (INGA-INDUSTRIES, 1968). The ore, which is syndepositional with the host rock, is composed of hematite, magnetite, carbonates, and quartz, and is variably covered with Meso-Cenozoic and Plio-Pleistocene sediments (Raucq, 1969). The mineral is banded (contrasting layers of 0.5–20 mm) and sometimes forms friable/solid crystallized flakes (INGA-INDUSTRIES, 1968). The BIF of this area are dated at ~2100 Ma (Raucq, 1969).

The analyzed hematite consists of lumps of relatively loosely attached tabular metallic flakes up to ~1 mm long (Fig. 1). The lumps were gently pestle-crushed or scraped into fine loose hematite flakes that were spread over normal-sized glass slides covered with a thin layer of synthetic fast glue. Under the binocular microscope, the flakes appeared metallic and black-reddish-brownish in color. Some flakes showed characteristic triangular surface markings of hematite basal forms. The glass slides were used for imaging and spectral analysis. The X-ray diffraction (XRD) analysis of samples ascertained a hematite composition.


**FIG. 1.** A general view of the hematite's partially loose and flakey composition on which the microbial-like structures (MLS) were found. The MLS are visible littering the surface of the larger plate on the upper left side of the image. The flakes reach up to 2 $\mu$m in length. SEM photomicrograph. Bar scale as indicated.

### *Analytical methods*

FE-SEM. The FE-SEM used for high-resolution imaging (1.2–3.0 nm at 15 and 1 kV, respectively) was a model JEOL JSM–7000F. Glass slides with hematite were sputter coated with gold-palladium and mounted on metal stubs.

SEM-EDX. The model employed was a JEOL Model JSM-6400. The X-ray detector (EDX) had a Si-Li crystal from Pioneer with a specific resolution of 138 eV. Some hematite samples were carbon coated and mounted on metal stubs. The software used for the interpretation of the spectra was Voyager Version 3.5 from Thermo-Noran.

FE-AES. The FE-AES used for surface analyses was a JEOL JAMP 9500F. An energy resolution $\Delta E/E$ of 0.06% was used. The spectra were obtained with a step of 0.1 eV. An electron beam of 10 kV and 1 nA at an angle of incidence of 30° with respect to the sample surface normally was applied. Before analysis, the materials were sputtered with the attached ion gun for several minutes with use of 1 keV $Ar^+$ ions to remove possible impurities. The spectra were corrected for the work function of the equipment ($e = 4.5$ eV). Scanning electron microscope (SEM) images were obtained via the secondary electron detector attached to the machine. The FE-AES, due to its high energy resolution, permits the discrimination between the different chemical states of a certain compound. Auger spectra were recorded on the studied microbial structures and on the background material for comparison; to avoid the influence of surface contaminations, sputtering was used to remove the outermost layers.

XRD analysis. Analyses were performed on several samples with increasing resolution and exposure time. Phase identification was based on powder diffraction patterns recorded with Siemens D500 diffractometer in the Bragg-Brantano geometry equipped with graphite monochromator and scintillation counter. Scans were collected via CuKa radiation (40 KV 30 mA) in the range 10–65° at a 2-$\theta$ step/time of 0.01°/10 s and 0.02°/7 s, respectively. The manually powdered hematite samples were placed in a common sample holder with the front loading cavity. XRD interpretation software was PDF-2 (Powdered Diffraction File-2) from The International Centre for Diffraction Data.

## Results

### *"Microbial-like" structures: forms and morphologies*

No extant microorganisms were seen on any examined samples. Instead, microbial-like structures (MLS) were detected in association with hematite planar surfaces. Based on their morphology, the MLS fall into two main categories: (1) coccoidal-like structures and (2) individual spheroidal forms (Fig. 2). Patterns of geometrical arrangement are formed by the chains; yet, in some instances, even single structures assume a certain geometric orientation.

Geometric chain arrangements: parallel and intersecting. Some of the MLS form chains that comprise visibly distinct 1 $\mu$m sized spheroids (Fig. 2a–d), often arranged in parallel (Fig. 2a). This geometrical arrangement occurs in pairs or multiple chains (Fig. 2a). Sometimes the parallel chains, though fused together, continue to maintain their individuality (Fig. 2a, 2c, 2d). Figure 2b shows a chain that reveals a secondary structure of distinct divisions formed at constriction points (if microbial, possibly representing septae). The number of spheroids in each of these divisions appears similar, usually five in number (Fig. 2b). Intersecting parallel chains create incomplete triangular forms with similar angles (~60°) and incipient concentric ones (Fig. 2c, 2d).

Non-oriented coccoidal-like structures. These are the most abundant MLS on hematite surfaces. The chains, made up of spheroidal structures, show budding-like globular protrusions (Fig. 3), dichotomous (Fig. 4), and sinusoidal forms (Fig. 5) that reach up to 25 $\mu$m in length and ~1 $\mu$m in diameter. In many instances, new globular appendages branch out from the main chain (Fig. 3a–i) and are connected by a narrowing ligature that creates a constriction at the site of incipient branching, which we term "necking" in the figures (Fig. 3a–e, 3h). Although not entirely clear, it seems that the new globular spheroids are formed at two different angles from the main body: at acute (*e.g.*, Fig. 3b) and right angles (*e.g.*, Fig. 3f).

Dichotomy occurs as simple and multiple branching at 30–90° from the main chain, making a typical V shape (Fig. 4a–f). The new branches are composed of multiple spheroids arranged as secondary chains that branch further (Fig. 4e–f). The branching sites often make nodes that are bigger than the rest of the chain (Fig. 4c, 4d, 4e). Surface texture of the chains is similar to that of the single spheroids. Coccoidal-like chains also show distinct sinuous forms with similar budding-like and branching features as the straight chains (Fig. 5a–d). Their sinuosity can be simple (Fig. 5a–b) or multiple (Fig. 5c–d). As seen in Fig. 5d, the chain-hematite surface contact line shows threads growing from the chain body onto the hematite surface (arrow).

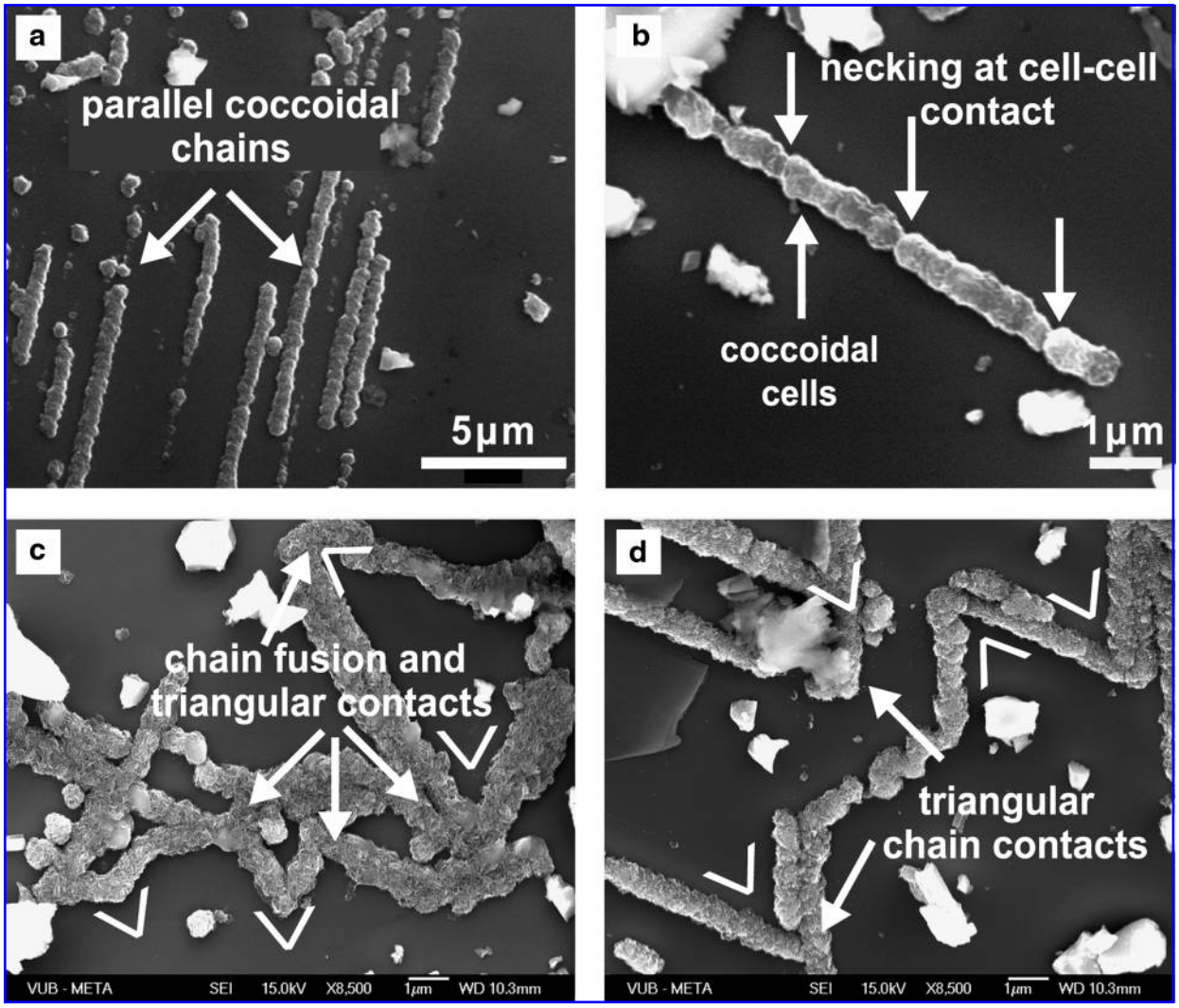


**FIG. 2.** Geometry of coccoidal-like chains (CLC): parallel and intersecting on hematite surface. (**a**) Coccoidal-like forms arranged in parallel chains of different lengths (5–15 $\mu$m) but stable diameter ($\sim$1 $\mu$m) separated by $\approx$2–3 $\mu$m distance. SEM photomicrograph. Bar scale as indicated. (**b**) A detailed CLC showing characteristic constriction at contacts, probably septae. Although the chains display a coccoidal-like arrangement which is clearly visible along the chain, the constriction at some points marks possible grouping (upper white arrows) in $\sim$5-spheroid groups. SEM photomicrograph. Bar scale as indicated. (**c**–**d**) FE-SEM photomicrographs showing coccoidal-like chain fusion and characteristic chains forming triangular contacts at intersections (white V shape). The triangular chain intersections could be induced by the MLS growth pattern if influenced by hematite crystal lattice. In all figures, the black background is the hematite surface. Bar scale as indicated.

Single-spheroid (globular) forms. Isolated spherical structures frequently cover the hematite basal plane surfaces (Fig. 6a). Their diameter generally does not exceed 1 $\mu$m (Fig. 6b–c). Although more-elongated single forms are present (Fig. 6d, 6e, 6h), they do not attain typical rod shapes but rather slight elongation in one direction yielding a tapered end (Fig. 6d, 6h). The single structures, when in chain formation, appear to be connected to each other by a narrowing ligature in between the cells (Fig. 6d, 6e, 6g, 6h). A few MLS also show appendages ($\sim$500 nm long) connected to one end (Fig. 6g–h and their insets).

The MLS surfaces (in chains as well as in single spheroids) display a spongy structure and texture (*e.g.*, Fig. 6b–c). In one instance (see Fig. 11b), however, a part of the chain appears to lack the spongy structure and texture when compared to the rest of the chain. Moreover, the FE-SEM examination of the spheroids revealed nanometer-sized crystals attached to their outer surface. The specific nature of these crystals was not defined, but EDX analyses showed a predominant Fe concentration on the MLS surface, which indicated Fe deposition and enrichment on the surface (Fig. 7a–b) or within the Fe-encrusted chain sheath. A detailed field emission auger electron spectroscopy analysis of Fe-encrusted MLS, compared to the hematite background, confirmed the presence of magnetite ($Fe_3O_4$) on those surfaces. This is discussed further below.

### *Metal speciation and biomineralization*

XRD and EDX analysis. The XRD results show hematite as the major phase (Fig. 8). However, a single strong peak at the 35.9° 2-$\theta$ shows the presence of wustite (FeO), which is

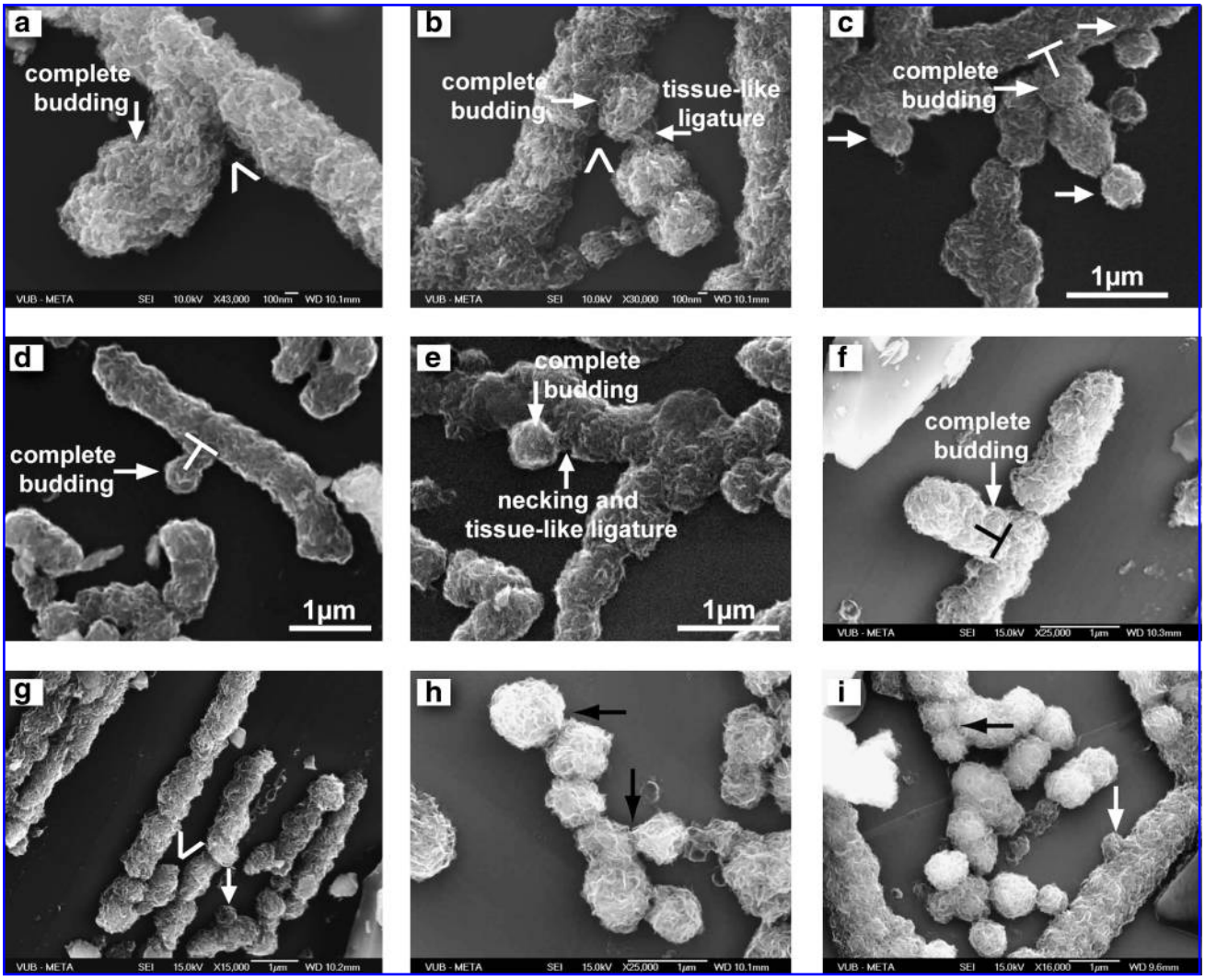


**FIG. 3.** Budding-like protrusions in non-oriented chains. Primary chains show spheroids budding in various stages of formation: complete (**a**–**f**) and incipient (unlabeled white arrows in c, **g**, i). The budding could form angular (V shape in a, b, g) or right-angle contacts (⊥ shape in c, d, f). Constriction with visible tissue-like ligature at the bud-mother chain contact is characteristic of most budding forms (b, c, e, and i). In figures (**h**–**i**) (black arrows) the arrangement of some "spheroidal" forms are suggestive, though not clearly, of a final stage of cellular-like division. SEM (c, d, e) and FE-SEM (a, b, f, g, h, i) photomicrographs. In all figures, the black background is the hematite surface. Bar scale as indicated.

attributed here as a surface precipitate on the MLS. This will be discussed further below. Here, the presence of magnetite is validated only by two weak peaks at the 35.5° and 43.5° 2-$\theta$. Although the XRD data (PDF-2, The International Centre for Diffraction Data, 2004) suggest the presence of these two minerals in addition to hematite, the absence of strong and other identifying peaks makes it difficult to assign their identity with certainty based on the XRD data alone. However, when EDX spectra (Fig. 7a, 7b) from the MLS and hematite background are also considered, the presence of Mg, Al, Si, and S traces only on the MLS, together with constant variations in Fe atomic percent (At%) and O At% on the two surfaces, indicates the presence of different mineral species. The chemical composition of the hematite surface, compared to the MLS, reveals a consistent general trend of lower Fe At% on the latter (*i.e.*, ~40–46 At%) versus the former (~50–60 At% Fe). Although these ranges were variable on other measurements, the difference in At% between the measurements on the hematite surface and MLS proved to be generally constant ~10–15 At%.

### *Field emission auger spectroscopy study*

Figure 9a shows a SEM image of the studied surface, with the analysis points indicated by their numbers. Figure 9b represents a typical oxygen KLL spectrum recorded for points on the MLS and hematite background, while Fig. 9c displays the Fe LMM spectra in both places. Both figures show a difference in peak shape between the spectra recorded in the different positions, located at the low-energy side of the spectrum. This indicates that the Fe-O compounds found at both positions are different in nature. In Fig. 9c, the Fe LMM spectrum recorded on a magnetite reference crystal can be found together with the spectra of hematite

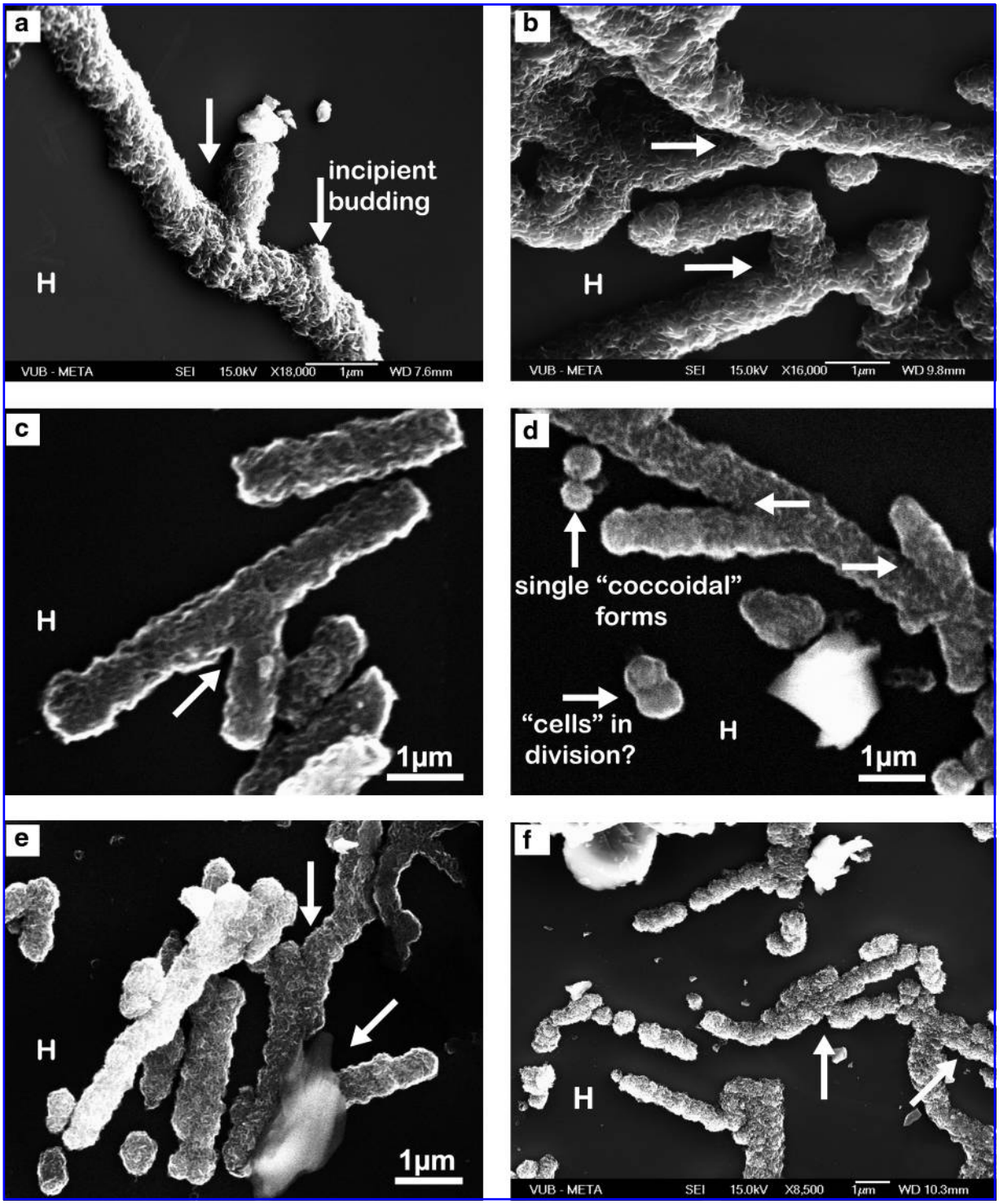


**FIG. 4.** Dichotomy in non-oriented CLC. CLC show characteristic dichotomy at different contact angles to mother chains: angular (white arrows: **a**–**f**) or right angle (**b**). The dichotomy could be a single secondary chain (white arrows: a, c) or multiple (white arrows: b–f). The coccoidal structure is well preserved in all instances. Other features such as incipient budding (a) and possible division (d) are also visible. FE-SEM (a, b, f) and SEM (c, d, e) photomicrographs. H is hematite surface. Bar scale as indicated.

background and the MLS. A positive correlation is observed between the spectrum obtained from the MLS and the magnetite reference. This clearly indicates that the MLS are encrusted with magnetite and possibly also wustite. Atomic percent of O and Fe were calculated (Table 1) from AES derivative spectra obtained from a sequence of points analyzed on hematite "flakes." The ratios indicate a general trend of Fe At% and O At% difference between the MLS and the hematite background (Table 1), which is similar to the trend of O At% and Fe At% from EDX analysis. The auger

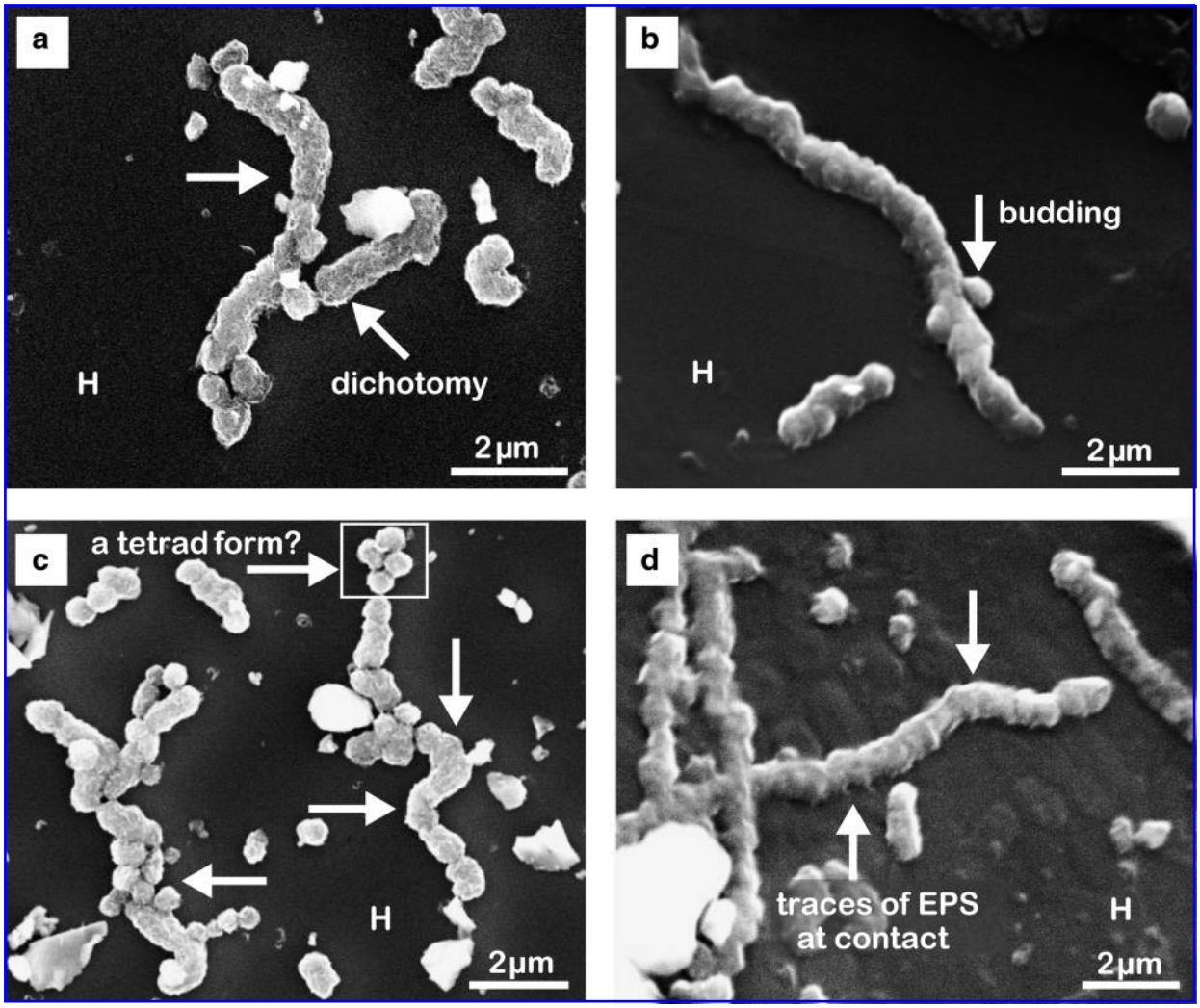


**FIG. 5.** Sinusoidal coccoidal chains. CLC showing simple (**a**, **b**) and multiple (**c**, **d**) sinusoidal forms (unlabeled white arrows). A possible tetrad arrangement of spheroidal forms can also be seen. All figures reveal additional characteristic features like budding and dichotomy. The typical external spongy texture of the surface is well preserved in (a) and (c). Traces of what can indicate an EPS are also visible at the chain-hematite surface contact line (d). SEM photomicrographs. H is hematite surface. Bar scale as indicated.

spectroscopy and EDX measurements confirmed the presence of C only as trace concentrations.

### *Attachment of MLS to the hematite surface*

Extracellular polymeric substance–like materials. As described above, SEM and FE-SEM images reveal evidence of direct adhesion and attachment of MLS to hematite surfaces. In several instances, the chains show fine threadlike appendages that extend transversally from the base of the chains toward the mineral surface. Morphologically, they form two distinct groups. The first (Fig. 10a–c) shows a quasi-regular pattern and generally does not extend far from the base of the chains except for the case in Fig. 10c, where a single bundle of threads ($0.05\times2\,\mu$m) extends to more than $2\,\mu$m from the chain and shows continuity, not only at the base, but also with the chain surface. Although not confirmed, these materials are best described as being similar to extracellular polymeric substances (EPS), the polymers that are extruded by living microbes and allow them to adhere onto solid substrata (*e.g.*, 10a–d and 11a, 11b) as a means of obtaining nutrients or energy from the underlying substrata (*e.g.*, Konhauser *et al.*, 1994, 2002b). Moreover, Fig. 10d shows dichotomous chains embedded in a background with a characteristic surface texture that display circular features and irregularities consistent with desiccated biofilms. Interestingly, other studies have documented that well-preserved fossil EPS and biofilms occur in association with hematite deposits, that is, the silicified biofilms from Barberton greenstone belt of South Africa (Westall *et al.*, 2000) and Gunflint iron formation (Allen *et al.*, 2001; Schelble *et al.*, 2004).

The second group of appendages (Fig. 11a–b) shows a network of relatively long and fine threads ($0.05\,\mu\text{m}\times4\,\mu$m), composed of 3–4 threads that directly extend from the hematite surface away from the base of the chain. In the lower right corner of Fig. 11b, these threads display smooth surfaces and rounded tips. For comparison with these figures and later discussion, Fig. 11c and 11d show modern *Geobacter*

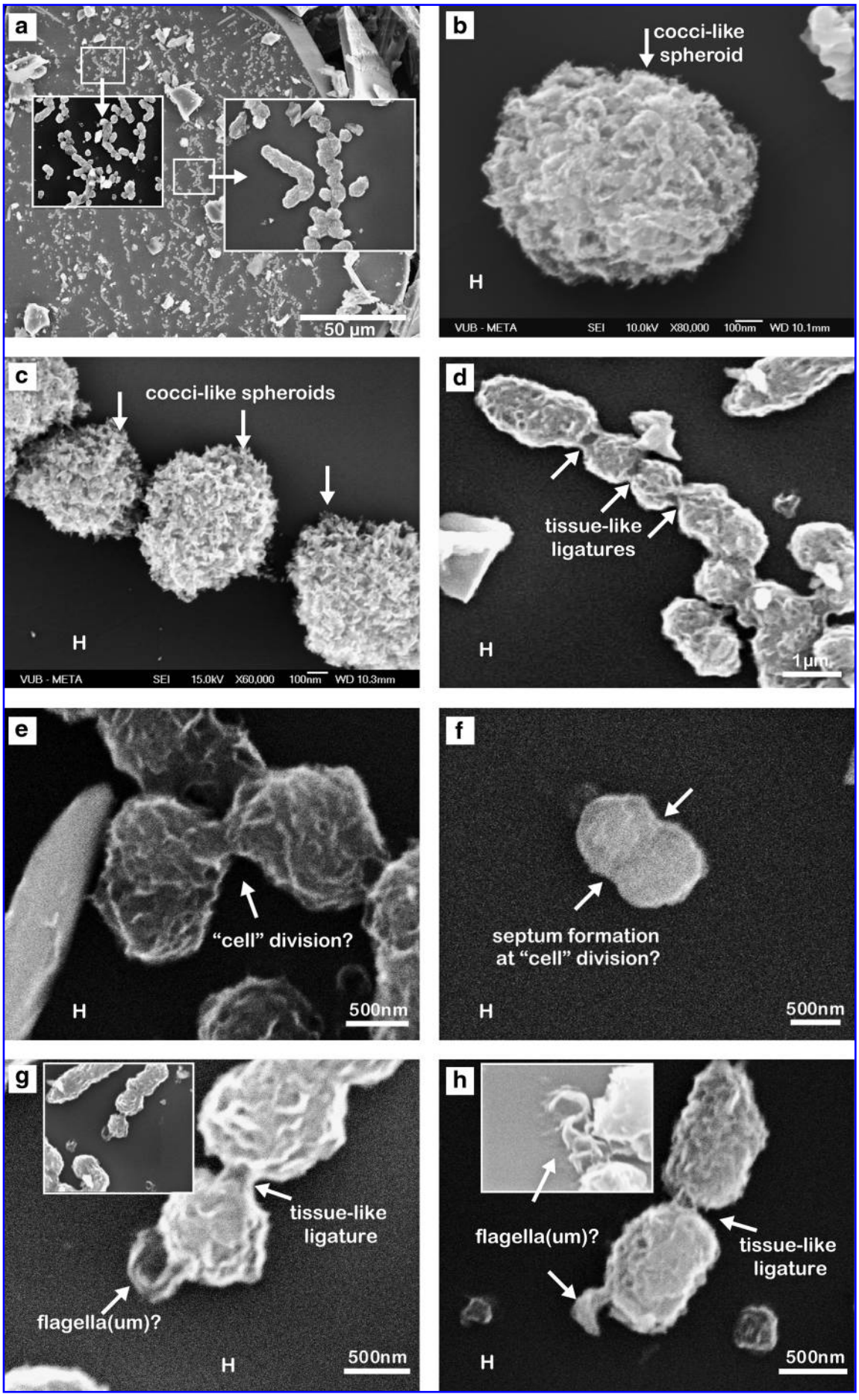
a
50 µm
b
cocci-like
spheroid
H
VUB - META SEI 10.0kV X80,000 100nm WD 10.1mm
c
cocci-like spheroids
H
VUB - META SEI 15.0kV X60,000 100nm WD 10.3mm
d
tissue-like
ligatures
H
1 µm
e
"cell" division?
H
500nm
f
septum formation
at "cell" division?
H
500nm
g
tissue-like
ligature
flagella(um)?
H
500nm
h
flagella(um)?
tissue-like
ligature
H
500nm

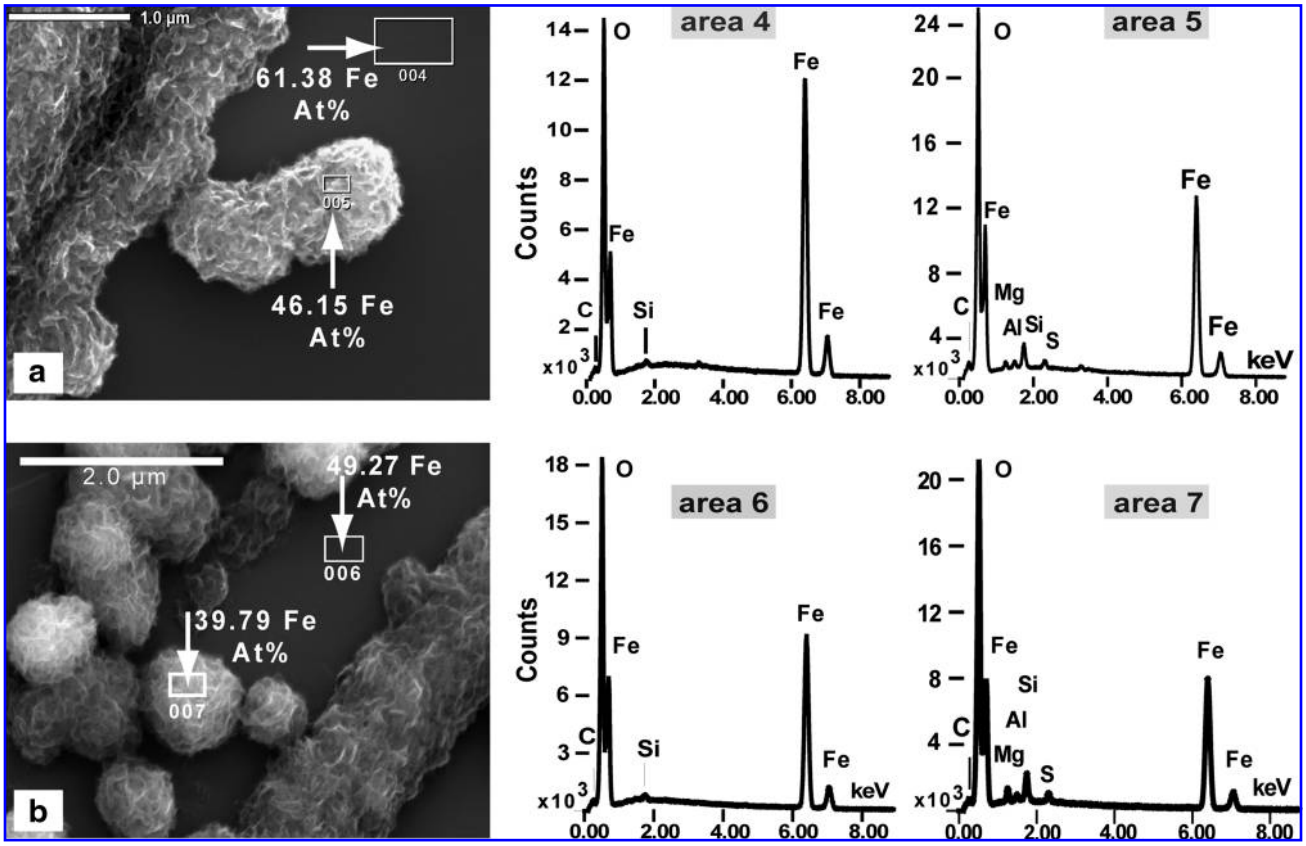


**FIG. 7.** EDX spectra and chemical composition of hematite surface compared to those from spheroidal forms. In both figures, the Fe At% in hematite exceeds that in the spheroids by approximately 10%. The spongy structure of the spheroids' surfaces is characteristically visible together with budding and coccoidal-like arrangement. FE-SEM photomicrographs. Bar scale as indicated.

*metallireducens* expressing a pili and flagella during hematite reduction (Childers *et al.,* 2002).

Circular pitting at contacts. Other observed features on the hematite include white-colored circular spots that appear as trace material on the hematite surface when the chains are dislocated or shifted from their original growth lines (Fig. 12a–d). SEM imaging showed that the circular spots are restricted to what likely were MLS attachment sites, that is, their chain alignment traces the previous presence of a chain with the circular spots, indicating sites on the hematite surface directly beneath the individual spheroids (Fig. 12a–b). These features (Fig. 12a) are not unlike the phenomenon of yeast cell budding scars (*e.g.*, Yeong, 2005). Other circular pits of visibly variable diameter (Fig. 12a, 12d, and inset) show clean surfaces and lack the whitish ring of attachment material.

### *Growth continuity*

Under the SEM, the hematite tabular flakes represented by variable basal planes often show fractured surfaces that are separated by linear gaps or simply lack physical contact. SEM imaging revealed single or clusters of chains bridging the fractures and gaps on the hematite surfaces by continuous growth across the gaps (Fig. 13a–d) and even chain overgrowth outside the mineral surface where it appears partially suspended (not shown). The bridging occurs across more than one gap and at variable height levels (Fig. 13b, 13d). In other instances (Fig. 13e), a secondary growth is superimposed upon a first one, which indicates two generations of spheroids at two successive growth instances. Cluster growth of MSL is also visible (Fig. 13f) where various MSL shapes are superimposed and form a cluster. Furthermore, in Fig. 13f another form of appendage is shown where a single and clearly contoured "pilus," imaged from above the plane surface, looks very similar to bacterial pili. The MLS body next to it (Fig. 13f) also reveals a curved appendage similar in form to others reported above.

It is also interesting to note that the inside of the MLS is more transparent than the surrounding background (Fig. 13b–d). This is especially evident where these forms lie across grooves and gaps in the surface. The edges of the form

**FIG. 6.** Single cocci-like forms littering the basal plane of hematite [(**a**) and the inset figures] and showing various features: typical single cocci-like spheroid (**b**, **c**) displaying spongy surface texture and Fe-enriched fine crystal growth on surface; tissue-like ligature and constriction between the spheroids (**d**, **g**, **h**); possible division (**e**, **f**) with clear septum formation (f); the appendages' form and position are similar to bacterial flagella [(**g**, **h**) and insets]. SEM and FE-SEM photomicrographs. H is hematite surface. Bar scale as indicated.

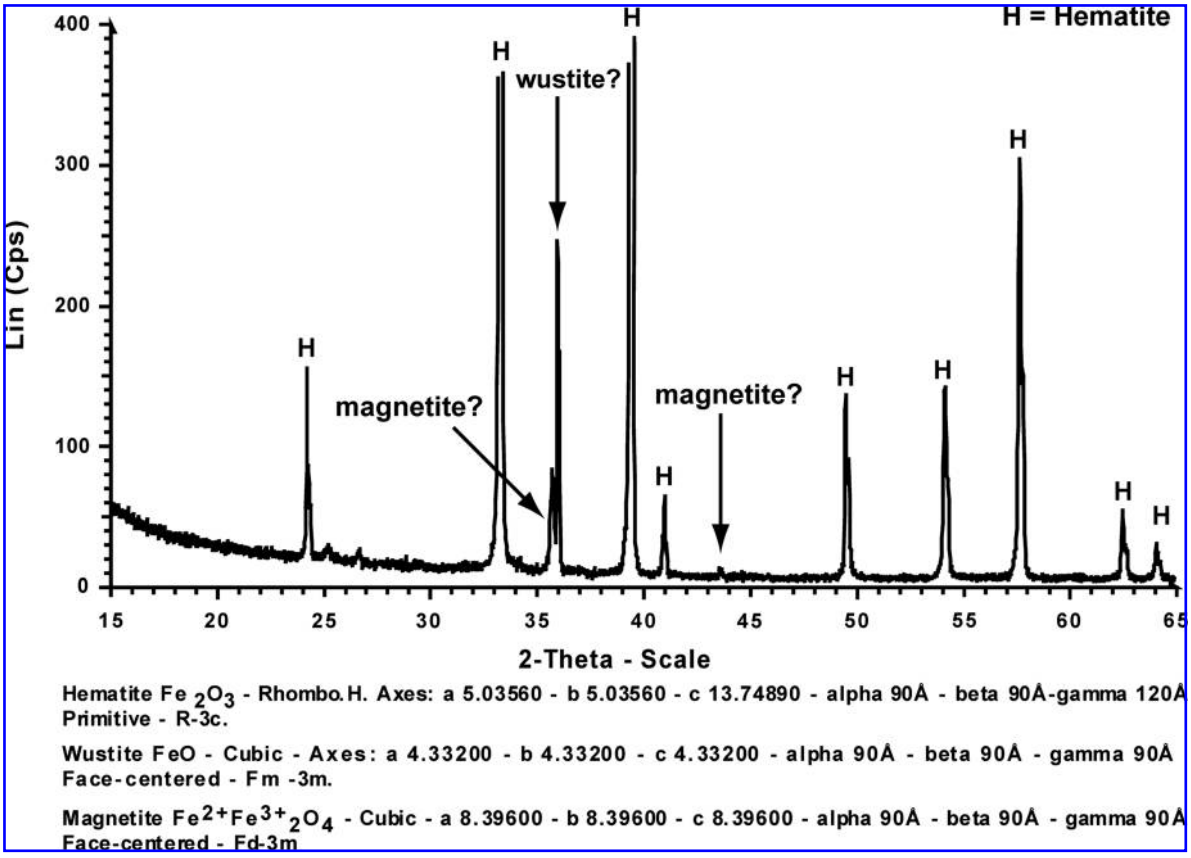


**FIG. 8.** XRD spectra showing that hematite ($\alpha$-$Fe_2O_3$) makes the major phase in analyzed samples. Single unascertained peaks at 2-$\theta$ 35.5°, 43.50°, and 35.9° suggest, nevertheless, the presence of magnetite ($Fe_3O_4$) and wustite (FeO), respectively.

show white, whereas the center is more transparent, which indicates that more material is present at the edges. This suggests, as will be discussed further below, that these forms are actually tubes that would, in any case, be consistent with our premise of a fossilized bacterial outer sheath.

## Discussion

In the absence of retrievable organic matter (due to extensive Fe encrustation), the only criteria available by which to assign a microbial origin for the MLS is based on morphology. Nevertheless, the collective presence of chains that are coccoidal in nature; single spheroids (termed "cocci" hereafter); spheroids undergoing apparent division and with appendages reminiscent of budding, sinuosity, dichotomous branching, branching angle, bridging, and growth continuity over fractures; mineralized surface textures; EPS-like material attaching the MLS to hematite surfaces; and possible nanowires lead us to conclude that the structures observed are consistent with a microbial origin.

### *Microbial attachment and pitting?*

Extracellular polymeric substance material is the main attachment mechanism by which bacteria adhere to a mineral surface (Little *et al.*, 1997). A few images (*e.g.*, Figs. 10, 11, and 13f) in this study clearly demonstrate a mechanism reminiscent of the microbial production of EPS. Moreover, other attachment mechanisms can be inferred from Fig. 12a–d, where the putative microbes employ spot attachment to certain sites on hematite surfaces (*i.e.*, the whitish rings at the hematite attachment sites envelop circular spots that appear as pits with $\varnothing = \sim 100$ nm). We suggest that these dissolution pits represent bacterial Fe(III) "reduction sites" on the hematite surface. Indeed, experimental studies (Grantham *et al.*, 1997; Rosso *et al.*, 2003; Gonzalez-Gil *et al.*, 2005) that have described bacterial interactions with iron oxides have shown dissolution pitting and etching of hematite surfaces associated with changes of the surface microtopography. Specifically, circular dissolution pitting was experimentally produced by *Shewanella putrefaciens* on $Fe^{3+}$ coated surfaces and interpreted as directly caused by bacterial Fe(III) reduction at the interface (Grantham *et al.*, 1997). Similarly, Rosso *et al.* (2003) demonstrated that *Shewanella putrefaciens* CN32 produced pitting on hematite surfaces at locations distinct from the points of bacterial attachment by way of electron-shuttling compounds during the reduction-dissolution process; yet, interestingly, the authors found no evidence to indicate reduction-dissolution at bacteria-mineral surface attachment sites. In a later experimental study (Lies *et al.*, 2005), it was demonstrated that *Shewanella oneidensis* reduced Fe(III) through "overlapping pathways" by combining reduction at a distance and direct contact to iron substrata.

In this study, other dissolution pits, aside from those apparently produced by direct bacterial contact, were not directly linked by position to the MLS attachment sites, and they lacked the whitish attachment ring and showed rather

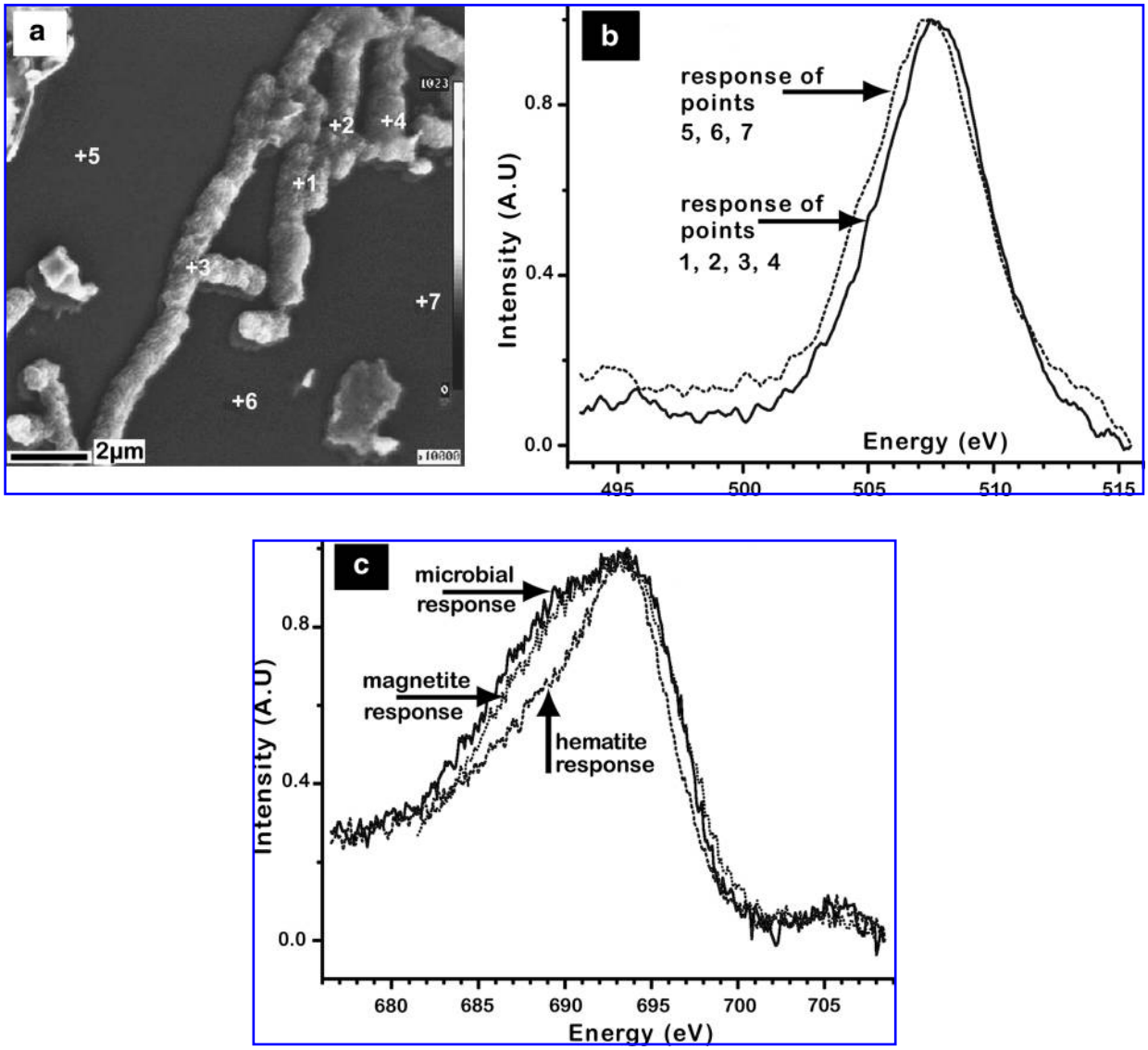


**FIG. 9.** Field emission auger electron spectroscopy analysis of selected points on the CLC and on the hematite surface. (**a**) SEM micrograph of analysis points on CLC. (**b**) Oxygen KLL auger spectrum signature of microbial and hematite response recorded at different sites on the surface. A shift in energy level (eV) is clearly visible between the two groups. (**c**) Fe LMM auger spectrum for the point groups. The spectrum recorded on a magnetite reference crystal is also shown. The spectra of CLC and of reference magnetite are clearly matching in energy level and intensity, while the hematite background is recording a different spectrum, which suggests encrustation by magnetite on the cocci-like spheroids. Bar scale as indicated. A.U., arbitrary units.

clean surfaces. However, their proximity to the chains and cocci calls for a comparison with the findings of Rosso *et al.* (2003) and suggests the possibility that the pitting on hematite surfaces is actually produced by direct microbial reduction at the microbe-hematite interface. Another experiment-based hypothesis concerning metal deposition and dissolution etching-pitting formation on hematite (001) and (*hk*0) surfaces, respectively, suggested that two distinct, though coupled, interfacial processes mediated through charge transport from the (001) to (*hk*0). This study also showed that the etch pits developed on various length scales with symmetry that corresponds to crystallographic orientation (Yanina and Rosso, 2008). In view of these novel findings, it is not possible to exclude the role of crystal surface specificity and crystallographic orientations in the microbial reduction of hematite and its association with secondary mineral formation and dissolution of original hematite substratum.

### *Formation of magnetite*

The Auger and XRD analyses results indicate the presence of ultrafine-grained (~10 nm) magnetite, possibly associated with a Fe(II) species (wustite?) and restricted to the surfaces of the MLS. The presence of two mineral species is also suggested by the calculated O/Fe atomic ratios from AES spectra (Table 1) and by the atomic O% and Fe% EDX values as measured on the MLS and on the hematite background

Table 1. Measured Values of O and Fe Atomic Percent Obtained by AES Method on Microbial Forms and Hematite Surface

| *Analysis point* | *Atomic O%* | *Atomic Fe%* | *O/Fe atomic ratio* | *Possible oxide* |
|---|---|---|---|---|
| Microbial forms | 56.78 | 43.22 | 1.32 | $Fe_3O_4$ |
| Microbial forms | 58.88 | 41.12 | 1.43 | $Fe_3O_4$ |
| Microbial forms | 58.97 | 41.03 | 1.44 | $Fe_3O_4$ |
| Microbial forms | 59.58 | 40.42 | 1.47 | $Fe_3O_4$ |
| Microbial forms | 55.23 | 44.77 | 1.23 | $Fe_3O_4$ |
| Microbial forms | 53.78 | 46.22 | 1.16 | FeO |
| Hematite surface | 59.65 | 40.35 | 1.48 | $Fe_2O_3$ |
| Hematite surface | 61.53 | 38.47 | 1.60 | $Fe_2O_3$ |
| Hematite surface | 63.57 | 36.43 | 1.74 | $Fe_2O_3$ |
| Hematite surface | 61.32 | 38.68 | 1.58 | $Fe_2O_3$ |
| Hematite surface | 61.05 | 38.95 | 1.56 | $Fe_2O_3$ |
| Hematite surface | 60.50 | 39.50 | 1.53 | $Fe_2O_3$ |

(Fig. 7a, 7b). The EDX measurements show a quasi-constant measured 10–15% difference in Fe%. This difference correlated well with the trend of calculated difference in AES O/Fe atomic ratios found on hematite and MLS. The AES trend of O/Fe atomic ratios also agreed with experimental measured O/Fe atomic ratios (Bizjak *et al.*, 2007) for hematite, magnetite, and FeO.

The occurrence of wustite can be genetically related to the presence of magnetite during the reduction of hematite under reducing conditions that are locally attainable at the microbe-hematite interface. Magnetite formation via dissimilatory Fe(III) reduction occurs in two discrete stages; the first is the actual reduction of ferric iron coupled to the oxidation of organic carbon and the subsequent epicellular release of $Fe^{2+}$, and the second is the reaction of ferrous ions with solid-phase iron oxides:

$$CH_3COO^- + 4Fe_2O_3 + 7H_2O \rightarrow 8Fe^{2+} + 2HCO_3^- + 15OH^- \quad (1)$$

$$2OH^- + Fe^{2+} + Fe_2O_3 \rightarrow Fe_3O_4 + H_2O \quad (2)$$

The magnetite "crystals" associated with the MLS suggest a similar process as above. Moreover, the Fe encrustation itself appears spongy in texture with no clear crystal structure. With high magnification of the encrusted surfaces, however, ultrafine "crystals" (~10 nm) are sometimes discernable (Fig. 6b), and their size agrees with published literature on biomineralized magnetite (10–50 nm; Bazylinski *et al.*, 2007). Apart from the strong indication that the magne-

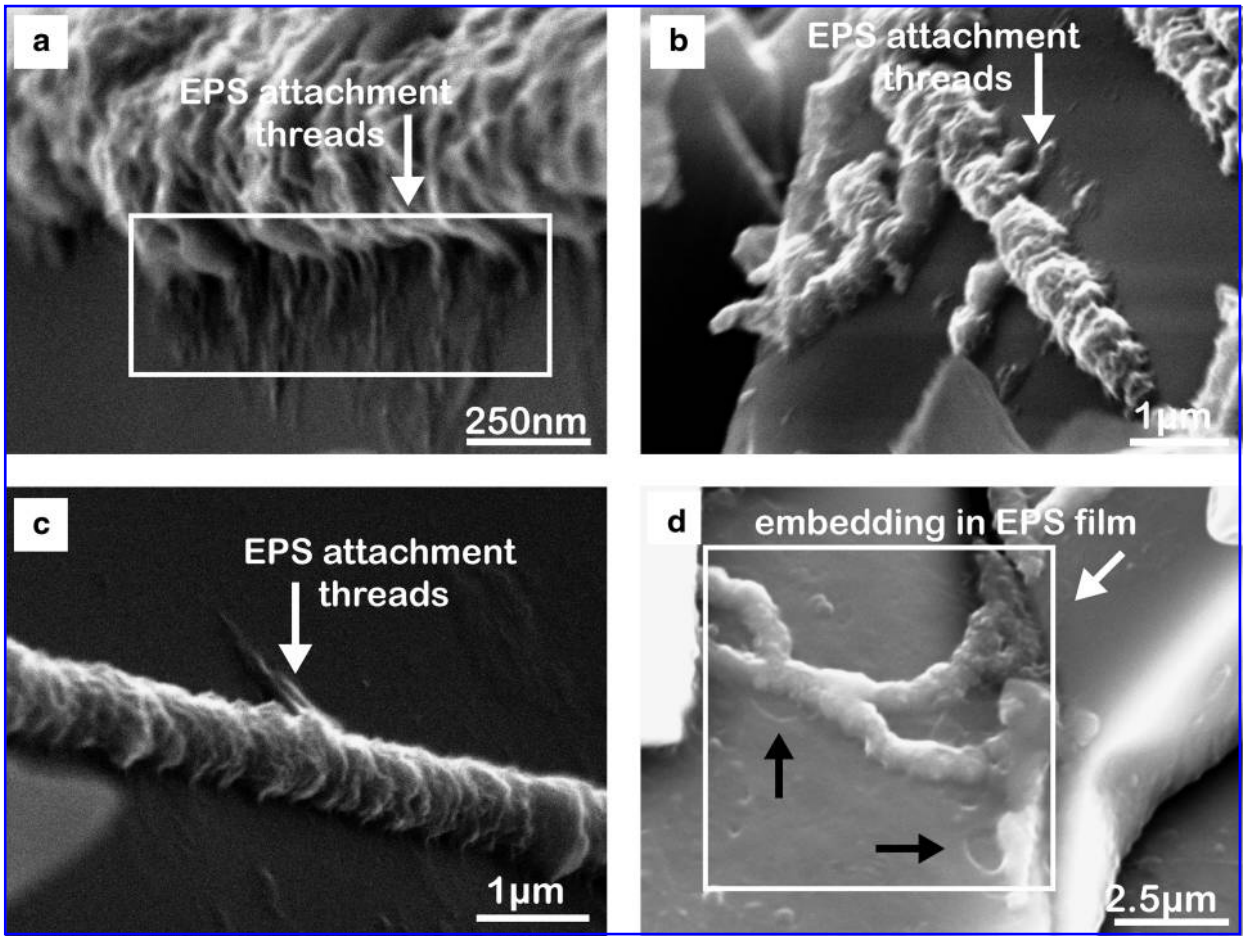


**FIG. 10.** MLS attachment to hematite surface. (**a**–**c**) Fine threads (white arrows) transversally spreading from the base of CLC on the hematite surface, forming thus a possible attachment mechanism. Similar threads of EPS are produced by modern bacteria to adhere to mineral surfaces. (**d**) shows (black arrows) sinuous and branching chains apparently embedded in EPS material with desiccation features resembling a "lunar" surface. SEM photomicrographs. Bar scale as indicated.

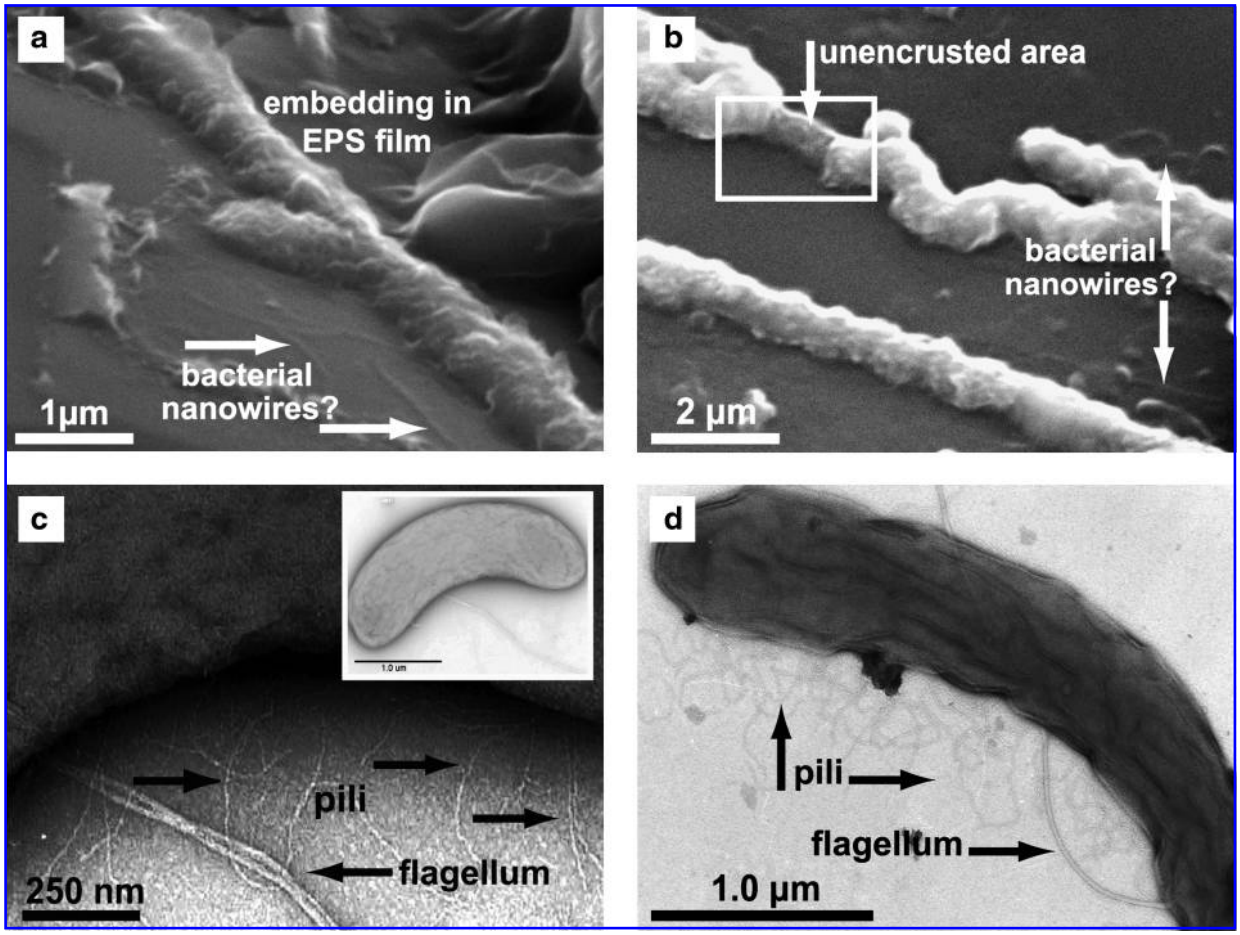


**FIG. 11.** MLS expressing pili "nanowires"? (**a**–**b**) show traces of a network of very fine (0.05 $\mu$m×4 $\mu$m) single threads (white arrows) extending on the hematite surface from the base of the coccoidal chain in a very similar manner to common bacterial pili in *Geobacter metallireducens* and *Shewanella oneidensis* strain MR-1. (**c**) and (d) show *G. metallireducens* expressing pili and flagella. The size and configuration of the potential pili and "nanowires" in (a) and (b) are comparable to those of *G. metallireducens* and possibly involved in adhesion to hematite surface. Also, the CLC in (a) appear embedded in an EPS film, and the sinusoidal chain in (b) (box) shows a part of the chain apparently lacking the mineral encrustation. SEM photomicrographs. Bar scale as indicated. [TEM images (c, **d**) courtesy of Dr. Susan E. Childers.]

tite is present on, or within, the Fe encrustation, it is difficult to show with certainty which of the two components of the Fe encrustation is responsible for the auger or XRD magnetite signals. However, the restricted association of magnetite and the possible other Fe(II) species to only the Fe encrustation on the MLS surfaces suggests a by-product formed through microbial dissimilatory reduction of the underlying hematite or by a reaction of the Fe(III) with the microbial biomass that was degraded during the fossilization process. In this regard, it has previously been suggested that extracellular magnetite accumulations characteristic of Fe(III)-respiring prokaryotes are associated with some of the putative fossilized microbes found in ancient martian meteorites (Richardson, 2000).

### *Hematite structure and bacterial geometric arrangement*

It is our contention that microbes can produce oriented growth forms and secondary iron oxide crystals that are influenced by the underlying mineral substratum composition and crystallography. Inorganic mineral growths on hematite surfaces have been studied in detail (Sunagawa, 1960a, 1960b, 1961, 1962a, 1962b, 1999, 2004; Sunagawa and Koshino, 1975). The natural Ångstroem spiral step heights on the hematite surface cannot be compared to the present micron-sized growths and to particulate linear and dendritic growths (Fig. 2a–b in Junta-Rosso *et al.,* 1996), though sometimes they bear resemblance in terms of their spiral growth geometry. These spiral forms, besides lacking the microbial morphology and structure of the present forms, do not posses the spongy texture specific of metal encrustation visible on many bacterial forms [compare Figs. 3, 4, and 6 to Figs. 19 and 24a in Little *et al.* (1997); to Fig.7d, 7e in Hansel *et al.* (2003); to Fig. 3a in Kappler and Straub (2005); and to Fig. 7a, 7b, 7c in Kappler *et al.* (2005)].

Hematite consists of octahedral layers of Fe-$O_6$ in coordinated hexagonal closest-packing perpendicular to the *c* direction (Fig. 14a). The electronic structure of the {001} surface is considered to have an Fe termination (Fig. 14b), though recent studies have shown evidence of oxygen and iron

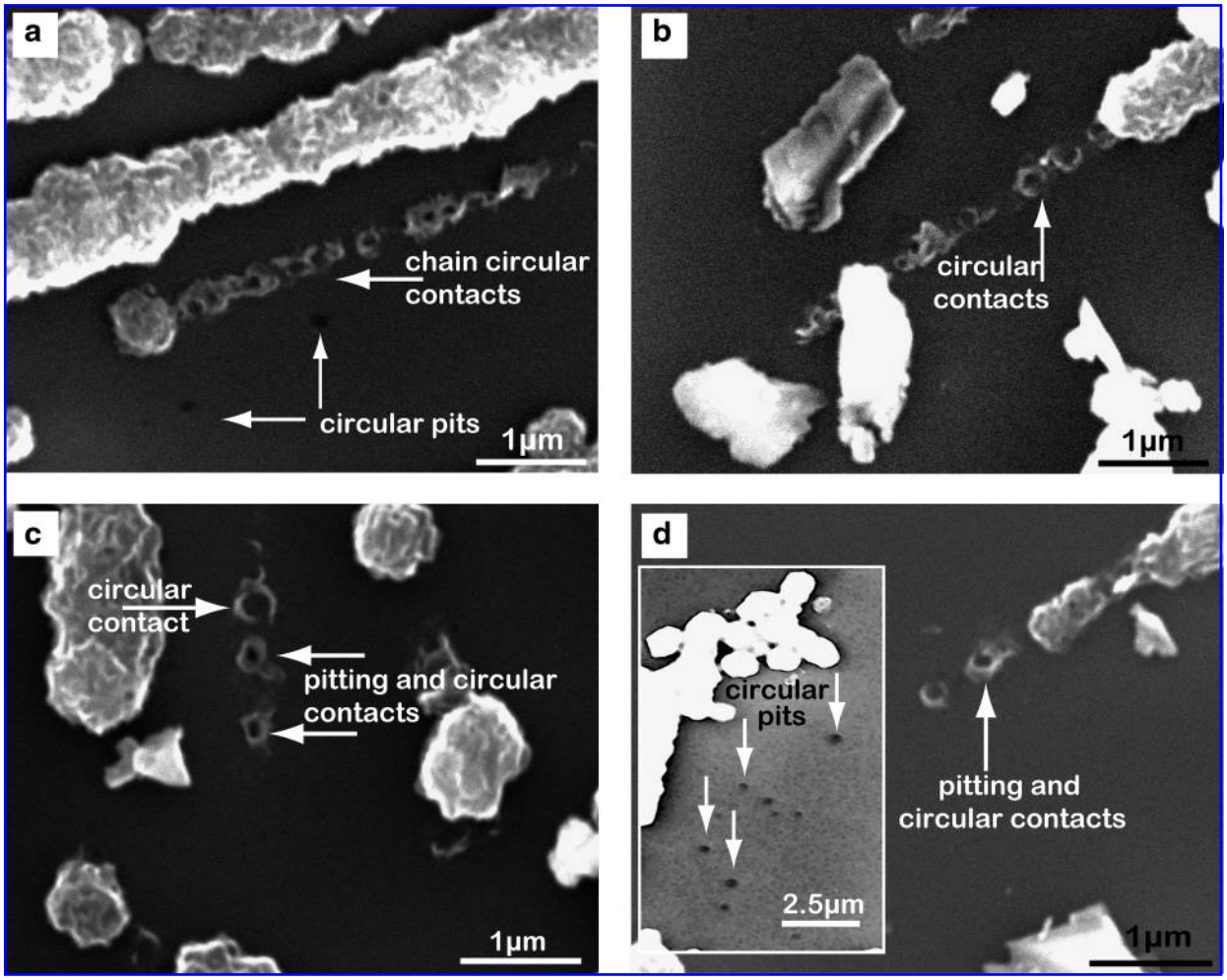


**FIG. 12.** Circular pitting and rings at MLS-hematite surface contact. Circular pits (Ø = 100 nm) and a ring of trace material marking previous MLS contact to the hematite surface. The pits are possibly formed due to a dissolution process. The circular pits and trace material in chain formation could be marking the position of original CLC (**a**, **b**). Also, the trace material on pits can be absent (a, b, and d inset figure). Single spheroids leave similar pits and trace material (**c**, **d**) as the coccoidal chains. The inset figure (d) is inserted from another image and is artificially enhanced for better pit visibility. SEM photomicrographs. Bar scale as indicated.

terminations coexistent on the {001} surface (Eggleston and Hochella, 1992; Becker *et al.*, 1996; Wasserman *et al.*, 1997; Eggleston, 1999; Thevuthasan *et al.*, 1999). These Fe terminations are characteristic of step and terrace heights (Fig. 14c) on the (001) hematite surface (Eggleston *et al.*, 2003). Previously, it was demonstrated that the Fe atoms, strongly coupled with bacterial donor heme groups, juxtaposed the (001) hematite surface (Neal *et al.*, 2003). Furthermore, the higher ferric site density of 4.2 $nm^{-2}$ on the (001) surface of hematite was found to be consistent with increased bacterial cell adhesion as opposed to lower density and cell adhesion to (100) and (111) surfaces of magnetite (Neal *et al.*, 2005). More-recent findings (Xiong *et al.*, 2006; Eggleston *et al.*, 2008) have confirmed the selective binding of *Shewanella oneidensis* outer-membrane *c*-type Cytochrome OmcA to hematite (001) surface that involved direct electron transfer. The FE-SEM images (Fig. 15a, 15b) reveal, on the hematite surfaces, steplike nanometer-sized lineaments on which the microbial forms grow and closely follow in alignment. It is suggested here that, in view of the electronic structure of hematite surfaces (as suggested by other previously mentioned studies), these MLS have the ability to grow and follow the higher Fe densities on the Fe terminations.

### *Nanowires?*

Based on modern analogues of *Shewanella oneidensis* and *Geobacter metallireducens* (Childers *et al.*, 2002; Reguera *et al.*, 2005; Gorby *et al.*, 2006), the presence of bacterial-like flagella (Fig. 6g, 6h, and inset) and potential "pili" and "nanowires" (Figs. 11a, 11b, and 13f) suggests a biological colonization of the hematite surface. Indeed, the putative bacterial "nanowires" in Fig. 11a and 11b are comparable in size and structure to those experimentally formed pili or nanowires associated with Fe(III)-reducing bacteria, such as *Shewanella oneidensis*, *Geobacter metallireducens,* and *G. sulfurreducens* (Childers *et al.*, 2002; Reguera *et al.*, 2005; Gorby *et al.*, 2006). Although these similarities do not confirm their nature and function as bacterial nanowires, their attachment to the bacterial cells on the hematite surface, as well as their apparent

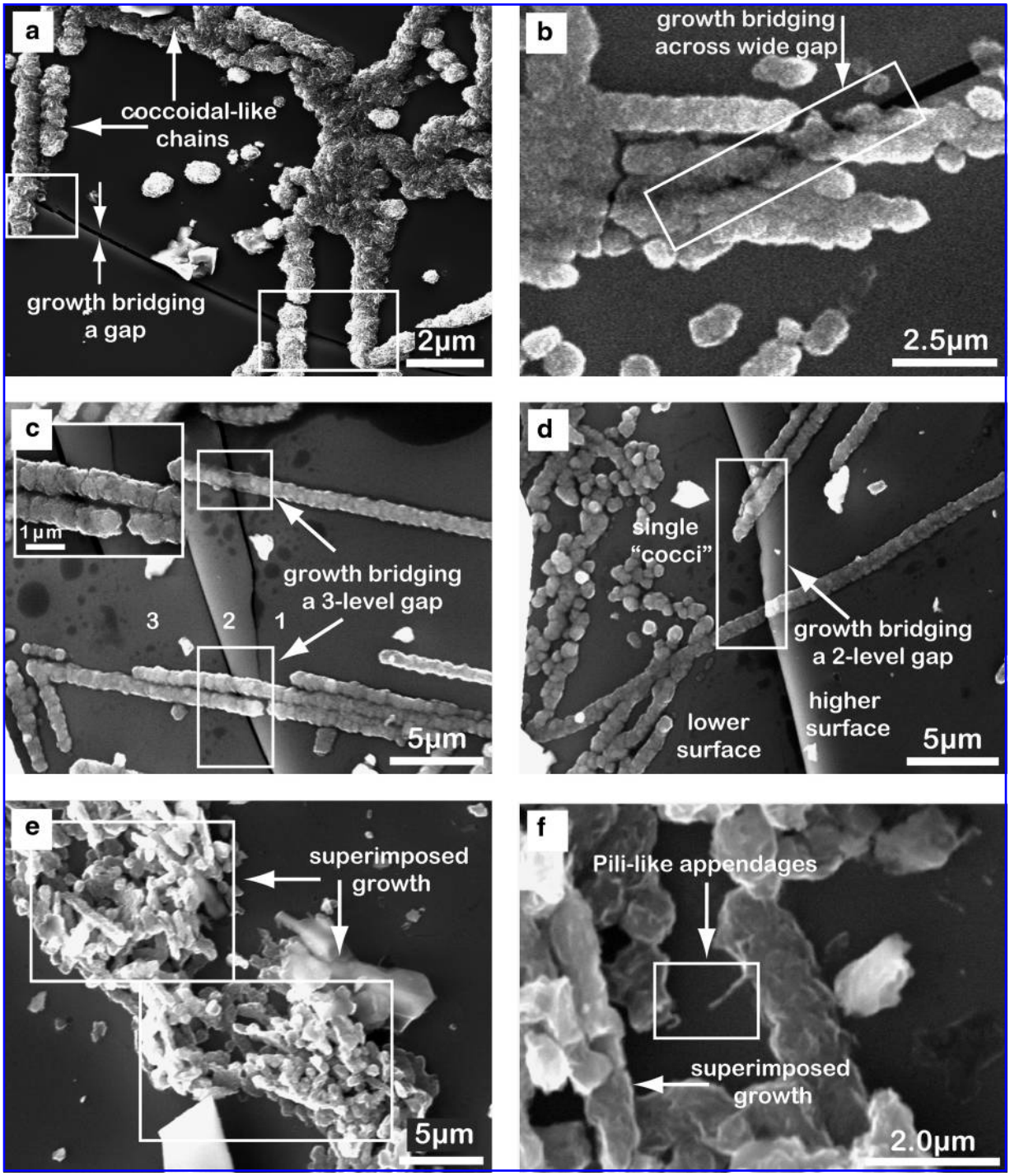


**FIG. 13.** Examples of MLS growth continuity across physical barriers on hematite surface. Bridging gaps of variable width in single or multiple chains and across variable surface heights (**a**–**d**). (c) and (d) show MLS growth across three-level and two-level surfaces, respectively. Interestingly, all the chains show no physical break in their forms, which indicates MLS growth that postdates the gap formation in addition to their superposition. In (c), the forms appear more transparent in the inside, particularly across the gap. The white edges of the forms and their more transparent centers indicate that more material is present at the edges, which suggests a tube structure. Figures (**e**) and (**f**) show MLS displaying superimposed growth on the hematite surface, possibly forming a colony? Furthermore, "pili-like" appendages extending from an MLS are clearly visible in (f). The growth form is comparable to hematite-encrusted bacteria reported by Kappler *et al.* (2005). SEM photomicrographs. Bar scale as indicated.

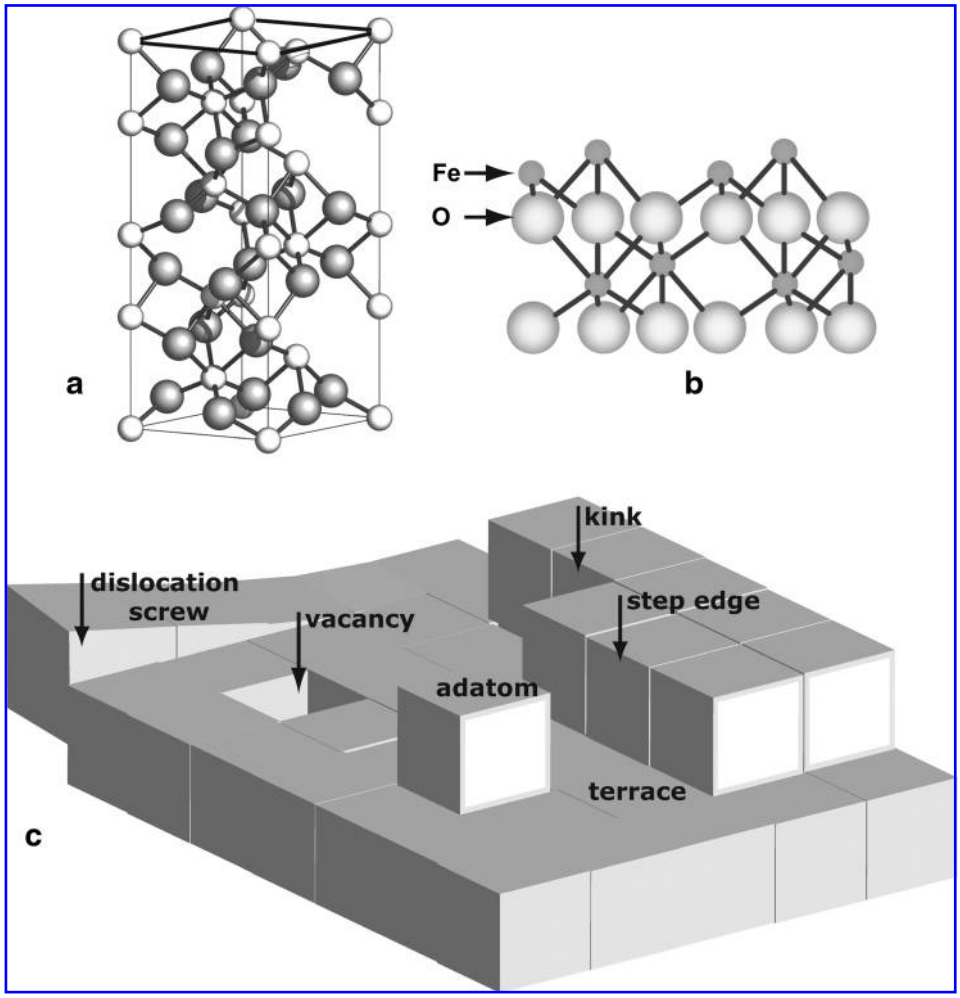


**FIG. 14.** Schematic structures of (**a**) bulk unit cell of hematite α-$Fe_2O_3$ showing the octahedral layers of Fe-$O_6$ in coordinated hexagonal closest-packing perpendicular to the *c* direction. (**b**) A doubly Fe-terminated hematite (001) surface. This Fe termination is considered to be involved in electron transfer between the iron-oxide surface and the bacterial outer membrane cytochromes during Fe(III) reduction, where some bacteria, for example, *Shewanella oneidensis*, were found to be specifically adhesive and dense on this surface. (**c**) A block diagram showing structural surface features of the hematite surface: kink, dislocation screw, vacancy site, terrace, step, and adatom. As high free-energy sites, these features are involved in iron oxide dissolution and reduction, both biotically and abiotically.

enshroudment in an EPS film that extends over the hematite surface, is consistent with a microbial origin. Furthermore, in Fig. 11a and 11b the "nanowires" appear not only to be attached to the coccoidal chain but also to exist between the two adjacent coccoidal chains, a fact that has been experimentally observed and assumed to facilitate electron transfer in the Fe(III) reduction process (Gorby *et al.*, 2006). These observations suggest that these "nanowires" may have played a similar role in the Fe(III) reduction and adhesion to hematite surfaces.

### *Fossilization*

Most microfossil preservation is typically associated with chert because the small grain size of the silica ideally templates the cellular structures (Konhauser *et al.*, 2003). By contrast, ferric-containing iron minerals are not typically associated with preservation due to the instability of Fe(III) and C during burial (metabolic reduction or metamorphism). Yet, although our assumption is purely speculative, we assume that the organic carbon that initially made up the biomass was oxidized. Some of that carbon may have ended up as fermentation products that then diffused away, while some of it was used by the Fe(III)-reducing bacteria (Konhauser *et al.*, 2005). They, in turn, used those electrons to reduce ferric iron to ferrous iron, with the end result being the formation of magnetite.

Until now, only a few studies have demonstrated the potential preservation of microbial cellular remains by iron oxides (*e.g.*, Dahanayake and Krumbein, 1986; Préat *et al.*, 2000; Schelble *et al.*, 2001; Geptner *et al.*, 2005). In these examples, the encrustation actually produced "biomorphic" structures that duplicated the bacterial and fungal filaments. Therefore, our observations of what appears to be "cellular" remains encrusted in magnetite are the first example of fossilization by a replacement process, where the organic structure acted as a template for mineral nucleation, after which it degraded and disappeared, leaving both a mineral cast and

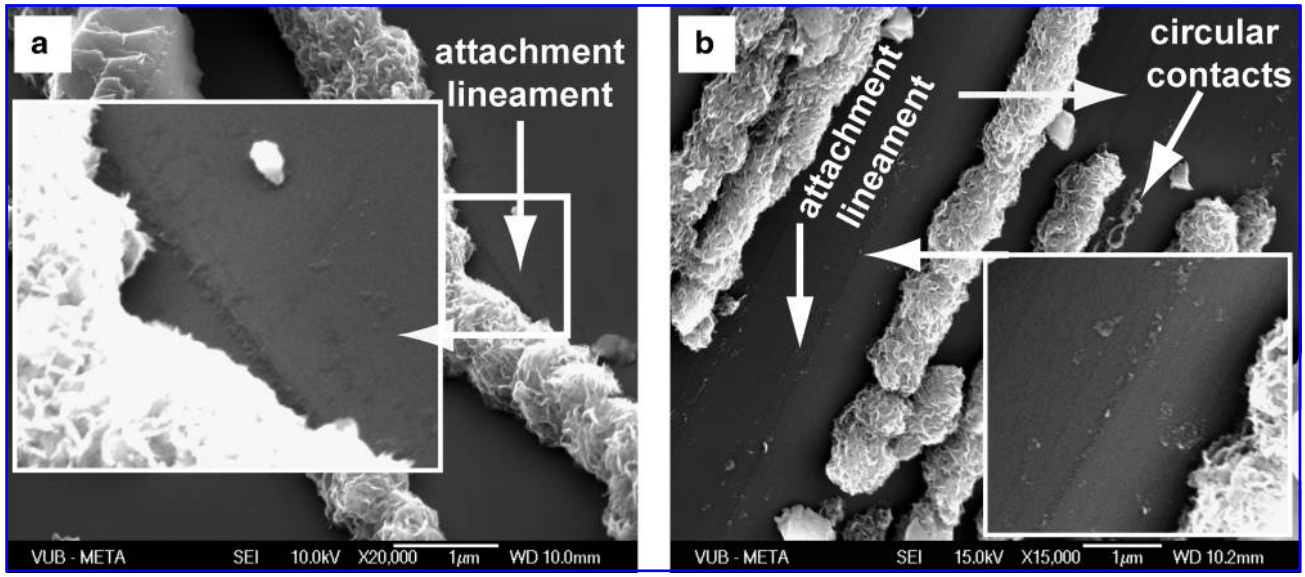


**FIG. 15.** Nanometer steplike lineaments on which the coccoidal chains of MLS are attached. It is possible, taking into consideration uniformity and parallelism of attachments, that these structural lineaments functioned as guides for the MLS attachment to the hematite surface. The inset figures are magnifications of the original lineaments. SEM photomicrographs. Bar scale as indicated.

crust. In this case, the biogenicity of our reported forms lies with the morphostructures created by the bacterial consortium (complexity, size, variable shapes, colonies, sinuosity, attachment, EPS material, budding, and branching), criteria some authors consider reliable enough to employ in the comparison of fossil bacteria with modern types to ascertain their biogenicity (Kazmierczak and Kremer, 2002).

One separate factor, which corresponds to the arguments for a biogenic origin, is the observation that under SEM and FE-SEM these microbial forms display a pattern that is consistent with very thin tube-like structures where the material is concentrated in the shell of a studied material and appears transparent at the center and more condensed and whitish at the sides when lying across a groove or a gap (Fig. 13c). The suggested tube structure of these microbial forms agrees with reports on ancient preserved tubular microbial forms (Schelble *et al.,* 2001; Schopf, 2006).

## Conclusions

Coccoidal-like chains of putative microbial origin found on natural hematite surfaces showed preferentially oriented growth patterns that may reflect an ability to recognize the crystal structure of the hematite substratum. Their adhesion to hematite is achieved through threadlike EPS material and by direct spot adhesion to the surface. The pitting found on hematite surfaces was attributed to this spot adhesion, which is interpreted here as representing "Fe(III) reduction sites." Collectively, the MLS are thus considered a fossil type of DIRB that are strongly associated with hematite as an electron acceptor. Despite our speculation, it is possible that the coccoidal-like forms represent microbes other than Fe(III) reducers and that the pits might have resulted from other reactions, such as dissolution via siderphores (iron-chelators). The evidence of magnetite encrustation on their surfaces further supports the notion that they are DIRB. Their fossil character was revealed by their total Fe mineralization and lack of retrievable organic carbon. The growth continuity on hematite surfaces also suggests a post-hematite formation, though in the absence of further data, it would be difficult to assign an age. Nonetheless, these findings imply that magnetite may in some instances be a proxy for ancient DIRB activity and, in that regard, help in the detection of life on ancient Earth and possibly other planetary bodies as well.

## Acknowledgments

The authors thankfully acknowledge the valuable assistance with laboratory facilities and technical advice from Prof. Jean Vereecken and Oscar Steenhaut, Department of Metallurgy, Electrochemistry and Materials Science/Vrije Universiteit Brussel, and Tiriana Segato, Department of Industrial Chemistry/Université Libre de Bruxelles. Kurt Konhauser would like to thank the Natural Sciences and Engineering Research Council of Canada for their financial support. We also thank the Royal Museum of Central Africa-Geological Research Institute-Brussels for kindly providing access to their geological and mineralogical database on BIF-Itabirites of Central Africa-Kasai region. Special thanks go to Dr. Susan E. Childers, Department of Geological Sciences, University of Idaho for kindly offering electron images of *Geobacter metallireducens*.

## Author Disclosure Statement

No competing financial interests exist.

## Abbreviations

At%, atomic percent; BIF, banded iron formations; CLC, coccoidal-like chains; DIRB, dissimilatory Fe(III)-reducing bacteria; EDX, X-ray detector; EPS, extracellular polymeric

substances; FE-AES, field emission auger electron spectrometer; FE-SEM, field emission scanning electron microscope; MLS, microbial-like structures; SEM, scanning electron microscope; XRD, X-ray diffraction.

## References


Allen, C.C., Westall, F.W., and Schelble, R.T. (2001) Importance of a martian hematite site for astrobiology. *Astrobiology* 1:111–123.

Bazylinski, D.A. and Frankel, R.B. (2003) Biologically controlled mineralization in prokaryotes. *Reviews in Mineralogy and Geochemistry* 54:217–247.

Bazylinski, D.A. and Moskowitz, B.M. (1997) Microbial biomineralization of magnetic iron minerals; microbiology, magnetism and environmental significance. *Reviews in Mineralogy and Geochemistry* 35:181–223.

Bazylinski, D.A., Frankel, R.B., Heywood, B.R., Mann, S., King, J.W., Donaghay, P.L., and Hanson, A.K. (1995) Controlled biomineralization of magnetite ($Fe_3O_4$) and greigite ($Fe_3S_4$) in a magnetotactic bacterium. *Appl. Environ. Microbiol.* 61:3232–3239.

Bazylinski, D.A., Frankel, R.B., and Konhauser, K.O. (2007) Modes of biomineralization of magnetite by microbes. *Geomicrobiol. J.* 24:465–475.

Becker, U., Hochella, M.F., Jr., and Apra, E. (1996) The electronic structure of hematite {001} surfaces: applications to the interpretation of STM images and heterogeneous surface reactions. *Am. Mineral.* 81:1301–1314.

Bizjak, M., Zalar, A., Panjan, P., Zorko, B., and Pracek, B. (2007) Characterization of iron oxide layers using Auger electron spectroscopy. *Appl. Surf. Sci.* 253:3977–3981.

Caccavo, F., Jr. and Das, A. (2002) Adhesion of dissimilatory Fe(III)-reducing bacteria to Fe(III) minerals. *Geomicrobiol. J.* 19:161–177.

Caccavo, F., Jr., Schamberger, P.C., Keiding, K., and Nielsen, P.H. (1997) Role of hydrophobicity in adhesion of the dissimilatory Fe(III)-reducing bacterium *Shewanella alga* to amorphous Fe(III) oxide. *Appl. Environ. Microbiol.* 63:3837–3843.

Canfield, E., Rosing, T., and Bjerrum, C. (2006) Early anaerobic metabolisms. *Philos. Trans. R. Soc. Lond., B, Biol. Sci.* 361:1819–1836.

Chaudhuri, S., Lack, J.G., and Coates, J.D. (2001) Biogenic magnetite formation through anaerobic biooxidation of Fe (II). *Appl. Environ. Microbiol.* 67:2844–2848.

Childers, S.E., Ciufo, S., and Lovley, D.R. (2002) *Geobacter metallireducens* accesses insoluble Fe(III) oxide by chemotaxis. *Nature* 416:767–769.

Croal, L.R., Johnson, C.M., Beard, B.L., and Newman, D.K. (2004) Iron isotope fractionation by Fe(II)-oxidizing photrophic bacteria. *Geochim. Cosmochim. Acta* 68:1227–1242.

Dahanayake, K. and Krumbein, W.E. (1986) Microbial structures in oolitic iron formations. *Mineralium Deposita* 21:85–94.

Das, A. and Caccavo, J.F. (2001) Adhesion of the dissimilatory Fe(III)-reducing bacterium *Shewanella alga* BrY to crystalline Fe(III) oxides. *Curr. Microbiol.* 42:151–154.

DiChristina, T.J., Moore, C.M., and Haller, C.A. (2002) Dissimilatory Fe(III) and Mn(IV) reduction by *Shewanella putrefaciens* requires *ferE,* a homolog of the *pulE* (*gspE*) Type II protein secretion gene. *J. Bacteriol*. 184:142–151.

DiChristina, T.J., Fredrickson, J.K., and Zachara, J.M. (2005) Enzymology of electron transport: energy generation with geochemical consequences. *Reviews in Mineralogy and Geochemistry* 59:27–52.

Edwards, K.J. and Rutenberg, A.D. (2001) Microbial response to surface microtopography: the role of metabolism in localized mineral dissolution. *Chem. Geol.* 180:19–32.

Edwards, K.J., Schrenk, M.O., Hamers, R.J., and Banfield, J.F. (1998) Microbial oxidation of pyrite: experiments using microorganisms from an extreme acidic environment. *Am. Mineral.* 83:1444–1453.

Edwards, K.J., Goebel, B., Rodgers, T.M., Schrenk, M.O., Cardona, M.M., Gihring, T.M., Hu, B., McGuire, M., Pace, N.R., Hamers, R.J., and Banfield, J.F. (1999) Environmental conditions, microbial populations, and the role of attachment in oxidative dissolution of pyrite at Iron Mt. *Geomicrobiol. J.* 16:155–179.

Edwards, K.J., Bond, P.L., Druschel, G.K., McGuire, M.M., Hu, B., Hamers, R.J., and Banfield, J.F. (2000) Geochemical and biological aspects of sulfide mineral dissolution: lessons from Iron Mountain, California. *Chem. Geol.* 169:383–397.

Eggleston, C.M. (1999) The surface structure of alpha-$Fe_2O_3$ (001) by scanning tunneling microscopy; implications for interfacial electron transfer reactions. *Am. Mineral.* 84:1061–1070.

Eggleston, C.M., and Hochella, M.F. (1992) The structure of hematite {001} surfaces by scanning tunneling microscopy: image interpretation, surface relaxation, and step structure. *Am. Mineral.* 77:911–922.

Eggleston, C.M., Stack, A.G., Rosso, K.M., Higgins, S.R., Bice, A.M., Boese, S.W., Pribyl, R.D., and Nichols, J.J. (2003) The structure of hematite ($\alpha$-$Fe_2O_3$) (001) surfaces in aqueous media: scanning tunneling microscopy and resonant tunneling calculations of coexisting O and Fe terminations. *Geochim. Cosmochim. Acta* 67:985–1000.

Eggleston, C.M., Vörös, J., Shi, L., Lower, B.H., Droubay, T.C., and Colberg, P.J.S. (2008) Binding and direct electrochemistry of OmcA, an outer-membrane cytochrome from an iron reducing bacterium, with oxide electrodes: a candidate biofuel cell system. *Inorganica Chim. Acta* 361:769–777.

Ewers, W.E. and Morris, R.C. (1981) Studies of the Dales Gorge Member of the Brockman Iron Formation, Western Australia. *Econ. Geol.* 76:1929–1953.

Frankel, R.B. and Bazylinski, D.A. (2003) Biologically induced mineralization by bacteria. *Reviews in Mineralogy and Geochemistry* 54:95–114.

Geptner, A., Ivanovskaya, T., and Pokrovskaya, E. (2005) Hydrothermal fossilization of microorganisms at the Earth's surface in Iceland. *Lithology and Mineral Resources* 40:505–520.

Gonzalez-Gil, G., Amonette, J.E., Romine, M.F., Gorby, Y.A., and Geesey, G.G. (2005) Bioreduction of natural specular hematite under flow conditions. *Geochim. Cosmochim. Acta* 69:1145–1155.

Gorby, Y.A., Yanina, S., McLean, J.S., Rosso, K.M., Moyles, D., Dohnalkova, A., Beveridge, T.J., Chang, I.S., Kim, B.H., Kim, K.S., Culley, D.E., Reed, S.B., Romine, M.F., Saffarini, D.A., Hill, E.A., Shi, L., Elias, D.A., Kennedy, D.W., Pinchuk, G., Watanabe, K., Ishii, S., Logan, B., Nealson, K.H., and Fredrickson, J.K. (2006) Electrically conductive bacterial nanowires produced by *Shewanella oneidensis* strain MR-1 and other microorganisms. *Proc. Natl. Acad. Sci. U.S.A.* 103:11358–11363.

Grantham, M.C., Dove, P.M., and DiChristina, T.J. (1997) Microbially catalyzed dissolution of iron and aluminum oxyhydroxide mineral surface coatings. *Geochim. Cosmochim. Acta* 61:4467–4477.

Hansel, C.M., Benner, S.G., Neiss, J., Dohnalkova, A., Kukkadapu, R.K., and Fendorf, S. (2003) Secondary mineralization pathways induced by dissimilatory iron reduction of ferrihydrite under advective flow. *Geochim. Cosmochim. Acta* 67:2977–2992.

INGA-INDUSTRIES. (1968) Prospection de minerai de fer au kasai. *Mission 1967–1968 par Paul Raucq, v.3, G 37. MRAC, Tervuren,* unpublished.

Jiao, Y., Kappler, A., Croal, L.R., and Newman, D.K. (2005) Isolation and characterization of a genetically tractable photoautotrophic Fe(II)-oxidizing bacterium, *Rhodopseudomonas palustris* strain TIE-1. *Appl. Environ. Microbiol.* 71:4487–4496.

Johnson, C.M., Beard, B.L., and Roden, E.E. (2008a) The iron isotope fingerprints of redox and biogeochemical cycling in modern and ancient Earth. *Annu. Rev. Earth Planet. Sci.* 36:457–493.

Johnson, C.M., Beard, B.L., Klein, C., Beukes, N.J., and Roden, E.E. (2008b) Iron isotopes constrain biologic and abiologic processes in banded iron formation genesis. *Geochim. Cosmochim. Acta* 72:151–169.

Junta-Rosso, J.L. and Hochella, J.M.F. (1996) The chemistry of hematite 001 surfaces. *Geochim. Cosmochim. Acta* 60:305–314.

Kappler, A. and Newman, D.K. (2004) Formation of Fe(III)-minerals by Fe(II)-oxidizing photoautotrophic bacteria. *Geochim. Cosmochim. Acta* 68:1217–1226.

Kappler, A. and Straub, K.L. (2005) Geomicrobiological cycling of iron. *Reviews in Mineralogy and Geochemistry* 59:85–108.

Kappler, A., Schink, B., and Newman, D.K. (2005) Fe(III) mineral formation and cell encrustation by the nitrate-dependent Fe(II)-oxidizer strain BoFeN1. *Geobiology* 3:235–245.

Kazmierczak, J. and Kremer, B. (2002) Thermal alteration of Earth's oldest fossils. *Nature* 420:477–478.

Kieft, T.L., Fredrickson, J.K., Onstott, T.C., Gorby, Y.A., Kostandarithes, H.M., Bailey, T.J., Kennedy, D.W., Li, S.W., Plymale, A., Spadoni, C.M., and Gray M.S. (1999) Dissimilatory reduction of Fe (III) and other electron acceptors by a *Thermus* isolate. *Appl. Environ. Microbiol.* 65:1214–1221.

Konhauser, K. (2007) *Introduction to Geomicrobiology*, Blackwell Publishing, Oxford.

Konhauser, K.O., Fyfe, W.S., Schultze-Lam, S., Ferris, F.G., and Beveridge, T.J. (1994) Iron phosphate precipitation by epilithic microbial biofilms in Arctic Canada. *Can. J. Earth Sci.* 31:1320–1324.

Konhauser, K.O., Hamade, T., Raiswell, R., Morris, R.C., Ferris, F.G., Southam, G., and Canfield, D.E. (2002a) Could bacteria have formed the Precambrian banded iron formations? *Geology* 30:1079–1082.

Konhauser, K.O., Schiffman, P., and Fisher, Q.J. (2002b) Microbial mediation of authigenic clays during hydrothermal alteration of basaltic tephra, Kilauea Volcano. *Geochemistry, Geophysics, and Geosystems* 3, doi:10.1029/2002GC000317.

Konhauser, K.O., Jones, B., Reysenbach, A.-L., and Renaut, R.W. (2003) Hot spring sinters: keys to understanding Earth's earliest life forms. *Can. J. Earth Sci.* 40:1713–1724.

Konhauser, K.O., Newman, D.K., and Kappler, A. (2005) The potential significance of microbial Fe(III) reduction during deposition of Precambrian banded iron formations. *Geobiology* 3:167–177.

Lies, D.P., Hernandez, M.E., Kappler, A., Mielke, R.E., Gralnick, J.A., and Newman, D.K. (2005) *Shewanella oneidensis* MR-1 uses overlapping pathways for iron reduction at a distance and by direct contact under conditions relevant for biofilms. *Appl. Environ. Microbiol.* 71:4414–4426.

Little, B.J., Wagner, P.A., and Lewandowski, Z. (1997) Spatial relationships between bacteria and mineral surfaces. In *Geomicrobiology: Interactions between Microbes and Minerals,* Vol. 35, edited by J.F. Banfield and K.H. Nealson, The Mineralogical Society of America, Washington DC, pp 123–159.

Lonergan, D.J., Jenter, H.L., Coates, J.D., Phillips, E.J., Schmidt, T.M., and Lovley, D.R. (1996) Phylogenetic analysis of dissimilatory Fe (III)-reducing bacteria. *J. Bacteriol.* 178:2402–2408.

Lovley, D.R. (1991) Dissimilatory Fe(III) and Mn(IV) reduction. *Microbiol. Mol. Biol. Rev.* 55:259–287.

Lovley, D.R. and Phillips, E.J.P. (1988) Novel mode of microbial energy metabolism: organic carbon oxidation coupled to dissimilatory reduction of iron or manganese. *Appl. Environ. Microbiol.* 54:1472–1480.

Lovley, D.R., Phillips, E.J.P., and Caccavo, F., Jr. (1992) Acetate oxidation by dissimilatory Fe (III) reducers. *Appl. Environ. Microbiol.* 58:3205–3208.

Lovley, D.R., Giovannoni, S.J., White, D.C., Champine, J.E., Phillips, E.J.P., Gorby, Y.A., and Goodwin, S. (1993) *Geobacter metallireducens* gen. nov. sp. nov., a microorganism capable of coupling the complete oxidation of organic compounds to the reduction of iron and other metals. *Arch. Microbiol.* 159:336–344.

Lovley, D.R., Holmes, D.E., and Nevin, K.P. (2004) Dissimilatory Fe(III) and Mn(IV) reduction. *Adv. Microb. Physiol.* 49:219–286.

Lower, S.K., Hochella, M.F., and Beveridge, T.J. (2001) Bacterial recognition of mineral surfaces: nanoscale interactions between *Shewanella* and α-FeOOH. *Science* 292:1360–1363.

Neal, A.L., Rosso, K.M., Geesey, G.G., Gorby, Y.A., and Little, B.J. (2003) Surface structure effects on direct reduction of iron oxides by *Shewanella oneidensis*. *Geochim. Cosmochim. Acta* 67:4489–4503.

Neal, A., Bank, T., Hochella, M., and Rosso, K. (2005) Cell adhesion of *Shewanella oneidensis* to iron oxide minerals: effect of different single crystal faces. *Geochem. Trans.* 6:77.

Nevin, K.P. and Lovley, D.R. (2002) Mechanisms for accessing insoluble Fe(III) oxide during dissimilatory Fe(III) reduction by *Geothrix fermentans*. *Appl. Environ. Microbiol.* 68:2294–2299.

Newman, D.K. and Kolter, R. (2000) A role for excreted quinones in extracellular electron transfer. *Nature* 405:94–97.

Préat, A., Mamet, B., De Ridder, C., Boulvain, F., and Gillan, D. (2000) Iron bacterial and fungal mats, Bajocian stratotype (Mid-Jurassic, northern Normandy, France). *Sediment. Geol.* 137:107–126.

Raucq, P. (1969) Les gisements d'itabirites de la region Luebo-Charlesville (Kasai). *Bulletin des Seances de l'Academie Royale des Sciences d'Outre-mer* 2:321–345.

Reguera, G., McCarthy, K.D., Mehta, T., Nicoll, J.S., Tuominen, M.T., and Lovley, D.R. (2005) Extracellular electron transfer via microbial nanowires. *Nature* 435:1098–1101.

Richardson, D.J. (2000) Bacterial respiration: a flexible process for a changing environment. *Microbiology* 146:551–571.

Roden, E.E. and Lovely, D.R. (1993) Dissimilatory Fe (III) reduction by the marine microorganism, *Desulfuromonas acetoxidans*. *Appl. Environ. Microbiol.* 59:734–742.

Rosso, K.M., Zachara, J.M., Fredrickson, J.K., Gorby, Y.A., and Smith, S.C. (2003) Nonlocal bacterial electron transfer to hematite surfaces. *Geochim. Cosmochim. Acta* 67:1081–1087.

Schelble, R.T., Westall, F., Allen, C.C., and Brearley, A.T. (2001) Hematite mineralized bacterial remains: implications for martian hematite deposits [abstract 1438]. In *32nd Lunar and Planetary Science Conference Abstracts,* Lunar and Planetary Institute, Houston.

Schelble, R.T., Westall, F., and Allen, C.C. (2004) ~1.8 Ga iron-mineralized microbiota from the Gunflint iron formation, Ontario, Canada: implications for Mars. *Adv. Space Res.* 33: 1268–1273.

Schopf, J.W. (2006) Fossil evidence of Archaean life. *Philos. Trans. R. Soc. Lond., B, Biol. Sci.* 361:869–885.

Sunagawa, I. (1960a) Mechanism of crystal growth, etching, and twin formation of hematite. *Mineralogical Journal* 3:59–89.

Sunagawa, I. (1960b) Growth history of hematite. *Am. Mineral.* 45:566–575.

Sunagawa, I. (1961) Step height of spirals on natural hematite crystals. *Am. Mineral.* 46:1216–1226.

Sunagawa, I. (1962a) Mechanism of growth of hematite. *Am. Mineral.* 47:1139–1155.

Sunagawa, I. (1962b) Mechanism of natural etching of hematite crystals. *Am. Mineral.* 47:1332–1345.

Sunagawa, I. (1999) Growth and morphology of crystals. *Forma* 14:147–166.

Sunagawa, I. (2004) Fundamentals and applications: a 50-year retrospective of the Japanese crystal growth community. *J. Cryst. Growth.* 264:631–638.

Sunagawa, I. and Koshino, Y. (1975) Growth spirals on kaolin group minerals. *Am. Mineral.* 60:407–412.

The International Centre for Diffraction Data. (2004) *Powder Diffraction File-2 (PDF-2),* Newtown Square, PA.

Thevuthasan, S., Kim, Y.J., Yi, S.I., Chambers, S.A., Morais, J., Denecke, R., Fadley, C.S., Lui, P., Kendelewicz, T., and Brown, G.E., Jr. (1999) Surface structure of MBE-grown $\alpha$-$Fe_2O_3$ (0001) by intermediate-energy X-ray photoelectron diffraction. *Surf. Sci.* 425:276–286.

Vargas, M., Kashefi, K., Blunt-Harris, E.L., and Lovley, D.R. (1998) Microbiological evidence for Fe(III) reduction on early Earth. *Nature* 395:65–67.

Wasserman, E., Rustad, J.R., Felmy, A.R., Hay, B.P., and Halley, J.W. (1997) Ewald methods for polarizable surfaces with application to hydroxylation and hydrogen bonding on the (012) and (001) surfaces of $\alpha$-$Fe_2O_3$. *Surf. Sci.* 385:217–239.

Westall, F., Steele, A., Toporski, J., Walsh, M., Allen, C., Guidry, S., McKay, D., Gibson, E., and Chafetz, H. (2000) Polymeric substances and biofilms as biomarkers in terrestrial materials: implications for extraterrestrial samples. *J. Geophys. Res.* 105:24511–24527.

Xiong, Y., Shi, L., Chen, B., Mayer, M.U., Lower, B.H., Londer, Y., Bose, S., Hochella, M.F., Fredrickson, J.K., and Squier, T.C. (2006) High-affinity binding and direct electron transfer to solid metals by the *Shewanella oneidensis* MR-1 outer membrane *c*-type Cytochrome OmcA. *J. Am. Chem. Soc.* 128:13978–13979.

Yanina, S.V. and Rosso, K.M. (2008) Linked reactivity at mineral-water interfaces through bulk crystal conduction. *Science* 320:218–222.

Yeong, F.M. (2005) Severing all ties between mother and daughter: cell separation in budding yeast. *Mol. Microbiol.* 55: 1325–1331.

Address correspondence to:
*Kamal Kolo*
*Vrije Universiteit Brussel*
*Department of Geology*
*Pleinlaan 2*
*1050-B, Brussels*
*Belgium*

*E-mail:* kakolo@vub.ac.be